Rheinisch-Westfälische Technische Hochschule Aachen (RWTH)

Analysis of the Spin Coherence Time at the Cooler Synchrotron COSY

von
Dennis Eversmann

Masterarbeit in Physik

vorgelegt der

Fakultät für Mathematik, Informatik und Naturwissenschaften
der RWTH Aachen

im Februar 2013

angefertigt am dritten physikalischen Institut B

bei

Professor Jörg Pretz

März, 2013

Ich versichere, dass ich die Arbeit selbstständig verfasst
und keine anderen als die angebenen Quellen und Hilfsmittel benutzt
sowie Zitate kenntlich gemacht habe.

Aachen, den

In particle physics the electric dipole moment (EDM) plays an important role, because it violates parity (P) conservation and time reversal (T) invariance. Under the assumption that the CPT symmetry is preserved by all physical phenomena, violation of the time reversal invariance implies CP violation.
The universe as we know it is dominated by baryons, which is unfolded by the dominance of matter observed by several experiments like COBE or WMAP [1]. The latter experiment observed a baryon asymmetry parameter of

$$\eta = \frac{n_B - n_{\bar{B}}}{n_\gamma} = (6.01 \pm 0.3) \cdot 10^{-10}. \tag{0.1}$$

In 1967 Andrei Sakharov formulated three necessary conditions of a baryon-generating interaction to produce more matter than antimatter:[2]

- Baryon number B violation
- C-symmetry and CP-symmetry violation
- Interactions out of thermal equilibrium

The standard model (SM) predictions for the EDM of nucleons are between 10^{-33} and 10^{-31} $\mathrm{e \cdot cm}$ [3] and therefore much too small to be detected with experiments which are planned in the nearer future. However, the CP violation in the SM is many orders of magnitude too small to explain the matter and anti-matter asymmetry in the universe, thus measuring an EDM not compatible with the SM could result into a better understanding of the matter dominated universe.

Over the years a lot of experiments searching for a non-vanishing EDM in systems without any electromagnetic charge, such as neutrons or atoms, were performed. One of the most ambitious attempts is the nEDM experiment at the Paul Scherrer Insitut, where ultra cold neutrons are used to measure an EDM of the magnitude 10^{-28} $\mathrm{e \cdot cm}$ [4]. Another attempt detecting SM violating EDMs can be realized by measuring spin shifts of charged particles stored in a storage ring. For this purpose, a new collaboration JEDI was founded to design possible precursor experiments at the COoler SYnchrotron COSY at Juelich and to study systematics of a future EDM experiment [5].

One important requirement to measure the small spin shifts in the horizontal plane due to an EDM effect is a long coherence time of the spin vectors of the particles in the beam. The subject of this thesis is to study and to discuss the spin coherence time (SCT) for different settings of COSY.

Contents

1 Introduction

The standard model of particle physics is very successful in describing the known elementary particles and their interactions. However, this framework is not able to explain important questions concerning the physical nature of observed processes like the violation of CP symmetry. Up till now, CP violation is the only known mechanism which could explain the matter-antimatter asymmetry observed in the universe. To resolve this problem speculative models were developed, which often included particularly symmetry breaking. A permanent electric dipole moment EDM of fundamental or non degenerated particles represents an excellent probe of physics beyond the standard model, e.g. super-symmetric extensions of the standard model (SUSY) [6].

1.1 EDM

The violation of parity P and time reversal T symmetry is illustrated in a figurative way in fig. 1.1. The symmetry breaking is understandable by aligning the magnetic dipole moment (MDM) μ to the hypothetical permanent electric dipole moment (EDM) d. Under parity transformation the EDM changes its direction but not the MDM, whereas under time reversal the behavior of the two quantities is the opposite way around. Since the resulting system is not symmetric to the initial system under P and T transformation, the two symmetries are violated due to the implementation of an EDM. Assuming also CPT symmetry, which is approved by all physical experiments till this day, breaking time reversal implies a violation of the combined symmetry CP.

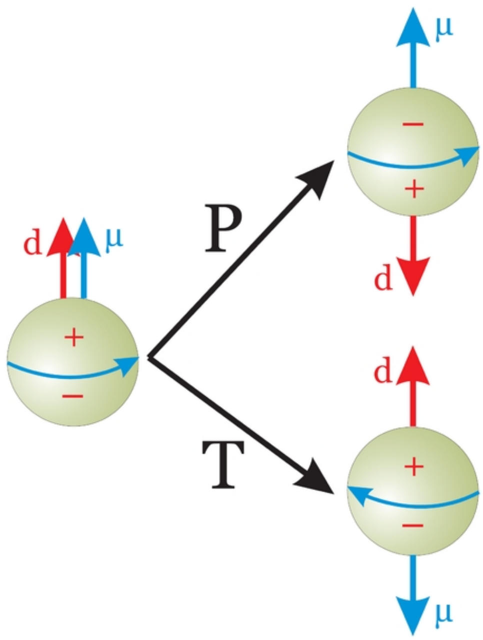

Figure 1.1: Illustration of the time reversal symmetry and parity breaking of a permanent particle EDM

In the standard model CP violation is included by the CP-violating complex phase in the CKM matrix and has been observed in several weak interaction experiments with neutral kaons [7] and B mesons [8] (in 2011 a first indication of CP violation in decays of neutral D mesons was published by LHCb). However, the amount of CP-violation is too small to be a candidate of explaining the baryogenesis in the early universe. The SM predictions of a proton or neutron EDM due to this CP-violation is in the order of $|d_{p,n}| \approx 10^{-32}\mathrm{e}\cdot\mathrm{cm}$, which is too small to be detected by experiments in the foreseen future. However, SUSY models generally lead to a large CP-violation, which would reveal an EDM in the range of $10^{-25}\mathrm{e}\cdot\mathrm{cm}$ and $10^{-28}\mathrm{e}\cdot\mathrm{cm}$.

Many experiments searching for a neutron EDM were performed in the last decades. In figure 1.2 the historical progression of the upper limit of the neutron EDM is shown with the predictions stemming from SUSY and the SM. The current upper limit value $10^{-26}\mathrm{e}\cdot\mathrm{cm}$ was published in 2006 by the Insitut Laue-Langevin in Grenoble, France [9]. As a result some parameters from SUSY models could be excluded or constrained and over the next 10 years experiments aiming at improving the upper limit down to a sensitivity of $10^{-28}\mathrm{e}\cdot\mathrm{cm}$.

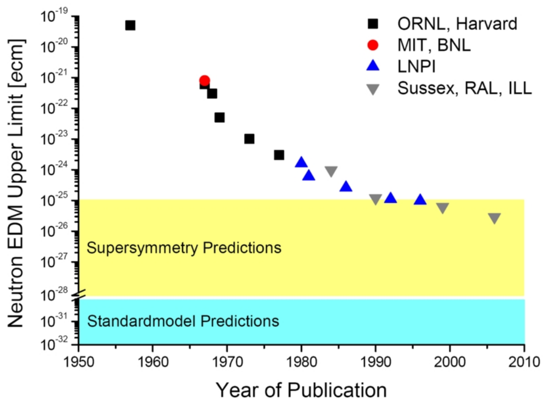

Figure 1.2: Upper limits of the neutron EDM with the predictions from SUSY and SM

Since the current upper limits of the proton EDM $d_p < 10^{-24}$ coming from experiments with ^{199}Hg-atoms [10], a direct measurement could improve the limit. Therefore two possible experiments were proposed. One at BNL to measure the EDM of a proton in a pure electric storage ring [11] and one at Forschungszentrum Juelich providing a electric and magnetic ring to investigate the EDM of protons, deuterons and helion [12]. Both potential experiments are designed to reach a sensitivity of $d \approx 10^{-29}\mathrm{e}\cdot\mathrm{cm}$. To push the upper limit to this level will not only trigger new constraints to SUSY, but also could improve our understanding of the QCD CP-violating $\overline{\Theta}$-parameter, which gives a value of the CP-violation in strong interactions. As there is no known reason of conserving CP in QCD, this is one important question in physics.

To perform an experiment with such a high sensitivity a lot of effort has to be done by studying systematics. The best place to do such investigations is the cooler synchrotron COSY at Forschungszentrum Juelich, which is introduced in the next chapter.

1.2 Cooler Synchrotron COSY

The COoler SYnchrotron COSY at Forschungszentrum Juelich is a middle energy storage ring with a beam momentum range from 0.3 to 3.7 GeV and a circumference of 183.4m. An overview of the storage ring is given in figure 1.3, where all external and internal components are shown.

Originally COSY was designed to study proton-proton interactions but nowadays it is also possible to store deuterons in the ring making it possible to carry out studies about systematics of the potential polarimetry which will be used for the final EDM ring. The important structures of COSY for studying such effects are the following:

- EDDA is the polarimeter to measure the polarization of the beam. It will be discussed in more detail in the following sections.
- Beam-cooling: COSY provides to methods to cool the beam (electron cooling and stochastic cooling), i.e. to reduce the emittance of the beam.
- Heating: The beam can be expanded in the horizontal plane by an electric dipole field providing stochastically particle momentum kicks.
- The polarized ion source provides polarized deuterons with a very good efficiency.
- Sextupole magnets are used to reduce the chromaticity of the beam and to increase the spin coherence time.
- The RF solenoid manipulates the spin of the particles in the beam.

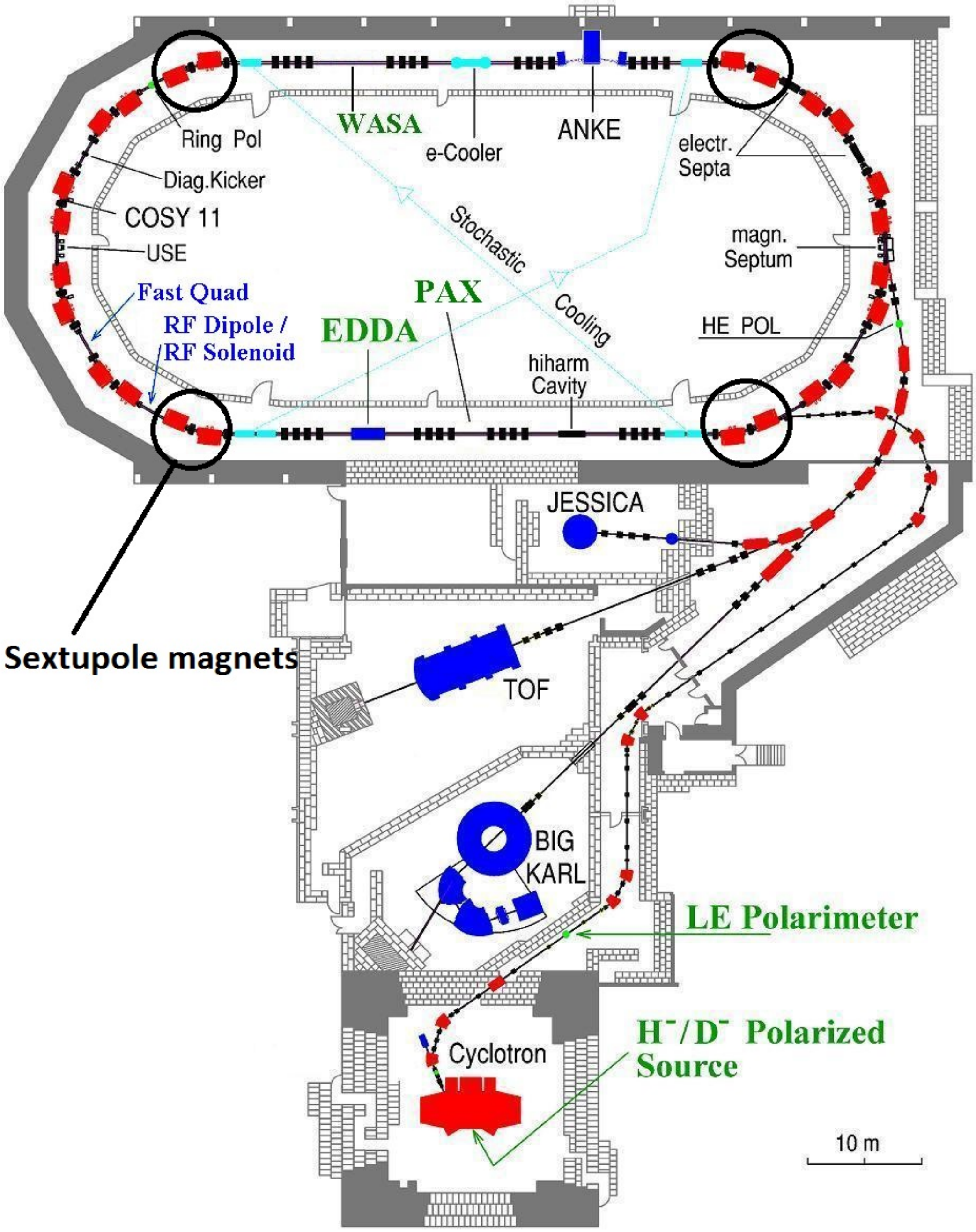

Figure 1.3: Schematic view of the COSY storage ring at Forschungszentrum Juelich.

2 Spindynamics in Storage Rings

2.1 Spindynamics

The spindynamic of a particle in a storage ring is determined by the external magnetic and electric field provided by the accelerator. In a planar ring the spin precesses about the vertical axis, while the vertical polarization of the particles is a conserved quantity. Due to the periodic influence of the electromagnetic forces on the particles one find energy depended spin resonances which can cause a depolarization of the polarized beam during the raising of the beam energy.

2.1.1 Magnetic and Electric Dipole Moment

In presence of a magnetic $\vec{B}$ and an electric $\vec{E}$ field the motion of the spin $\vec{S}$ of a charged particle at rest is given by [13]:

$$\frac{d\vec{S}}{dt} = \vec{\mu} \times \vec{B} + \vec{d} \times \vec{E} \tag{2.1}$$

The magnetic moment $\vec{\mu}$ and the EDM vector $\vec{d}$ are proportional to and aligned along the direction of the particle spin.

$$\vec{\mu} = g\frac{q}{2m}\vec{S} \tag{2.2}$$

$$\vec{d} = \eta\frac{q}{2m}\vec{S} \tag{2.3}$$

The proportional factor for the magnetic moment consists of the mass of the particle m, the electric charge q and the Landé g-factor. The quantity η in the EDM expression is analogous to the g value for the magnetic dipole moment. Furthermore the EDM vector $\vec{d}$ is proportional to the charge of the particle q and inversely proportional to the mass m.

For a point-like particle with spin $s = \frac{1}{2}$ the Dirac equation provides $g = 2$. Due to contributions of quantum mechanical corrections, expressed by Feynman diagrams with loops, additional contribution to the magnetic moments occur for elementary particles. The difference is called the anomalous magnetic moment, denoted as G and defined as:

$$G = \frac{g-2}{2} \tag{2.4}$$

For an electron G is very small ($G = 0.00115967$) [14], whereas composite particles like hadrons often have a huge anomalous magnetic moment originating from the gluon-quark interactions. The following table shows the G-values for protons, deuterons and helion:

	G	g
proton	1.7928	5.5856
deuteron	-0.1429	1.7142
helion	-4.1839	-6.3678

2.1.2 Thomas Bargmann-Michel-Telegdi (T-BMT) Equation

The spin motion in a magnetic field is determined by

$$\frac{d\vec{S}}{dt} = g\frac{q}{2m}\vec{S} \times \vec{B}. \tag{2.5}$$

applied in the Center-of-Mass System CMS of the particle. For spin calculations in storage rings this formula is not suitable, because the magnetic fields are known in the laboratory system. The transformation of the magnetic field into the laboratory frame yields to the Thomas-BMT equation [15]:

$$\frac{d\vec{S}}{dt} = \vec{S} \times \vec{\Omega}_{T-BMT} \quad \text{with} \tag{2.6}$$

$$\vec{\Omega}_{T-BMT} = \frac{q}{m}\left[\left(G + \frac{1}{\gamma}\right)\vec{B}_\perp + \frac{1+G}{\gamma}\vec{B}_\parallel - \left(G + \frac{1}{\gamma+1}\right)\vec{\beta} \times \vec{E}\right] \tag{2.7}$$

where $\gamma = \frac{1}{\sqrt{1-\beta^2}}$ describes the Lorentz energy factor, $\vec{B}_\perp$ and $\vec{B}_\parallel$ are the magnetic field components perpendicular and parallel to the momentum of the particle. $\vec{\Omega}$ represents the angular velocity of the spin precession. If one only takes into account transverse magnetic fields in the ring ($\vec{\beta} \cdot \vec{B} = 0$) the angular precession simplifies to:

$$\vec{\Omega}_{T-BMT} = \frac{q}{m}\left[\left(G + \frac{1}{\gamma}\right)\vec{B} - \left(G + \frac{1}{\gamma+1}\right)\vec{\beta} \times \vec{E}\right] \tag{2.8}$$

2.1.3 Spin Precession extended by EDM

The equation of the spin motion with allowance for the EDM can be obtained by modifying the T-BMT equation.

$$\vec{\Omega} = \vec{\Omega}_{T-BMT} + \vec{\Omega}_{EDM} \tag{2.9}$$

$$\vec{\Omega}_{EDM} = \eta\frac{q}{2m}\left(\vec{E} - \frac{\gamma}{\gamma+1}\vec{\beta}(\vec{\beta} \cdot \vec{E}) + \vec{\beta} \times \vec{B}\right) \tag{2.10}$$

If rf cavities are not used ($\vec{\beta} \cdot \vec{E} = 0$), the parallel electric field component is neglectable thus the term for the spin precession induced by an EDM simplifies to:

$$\vec{\Omega}_{EDM} = \eta \frac{q}{2m} \left(\vec{E} + \vec{\beta} \times \vec{B} \right) \tag{2.11}$$

Finally the angular velocity of the spin precession for vanishing parallel electric and magnetic fields yields to:

$$\vec{\Omega} = \frac{q}{m} \left[\left(G + \frac{1}{\gamma} \right) \vec{B} - \left(G + \frac{1}{\gamma + 1} \right) \vec{\beta} \times \vec{E} + \frac{\eta}{2} \left(\vec{E} + \vec{\beta} \times \vec{B} \right) \right] \tag{2.12}$$

Based on this formula several experimental methods for measuring the EDM can be derived, but one has to take into account that the effect of the EDM in ordinary electromagnetic storage rings is small compared to the influence of the magnetic dipole moment.

2.1.4 Invariant Spin Field

The invariant spin field $\vec{n}(\vec{z}, \theta)$ depends on the position $\vec{z} = (x, y, z, p_x, p_y, p_z)$ of the particle in the six-dimensional phase-space and the azimuthal position θ in the ring. The invariant spin field is a special solution to the Thomas-BMT equation 2.8 with the property that

$$\vec{n}(\vec{z}, \theta + 2\pi) = \vec{n}(\vec{z}, \theta). \tag{2.13}$$

A particle with the initial spin $\vec{S}_i$ at the phase-space position $\vec{z}_i$ has the final spin $\vec{S}_f$ after it has been transported to the phase-space point $\vec{z}_f$ during one turn in a circular storage ring. If $T_{t=1}$ is the spin transfer matrix for one turn, it exists a spin field vector $\vec{n}(\vec{z}_i, \theta)$ for every phase-space point $\vec{z}_i$ such that

$$\vec{n}(\vec{z}_f, \theta) = T_{t=1}(\vec{z}_i, \theta) \vec{n}(\vec{z}_i, \theta). \tag{2.14}$$

For a reference particle with $\vec{z}_i = \vec{z}_f = 0$ the corresponding invariant spin field vector is usually called invariant spin axis or the spin closed-orbit $\vec{n}_0(\theta)$.

2.2 Techniques for EDM Searches in Storage Rings

2.2.1 Siberian Snake as a Spin Rotator

A Siberian snake provides a stable longitudinal spin-closed orbit in a target section opposite the snake [13]. In figure 2.1 the concept of a proton EDM measurement using a Siberian snake is shown. The spin-closed orbit is aligned along the direction of motion of the beam in the straight section opposite the snake (top panel). In the middle and lower panel one sees additional electric radio frequency RF E-field systems in front and behind the snake. Due to the torque $\vec{d} \times \vec{E}$ a certain degree of depolarization arises which is proportional to the EDM.

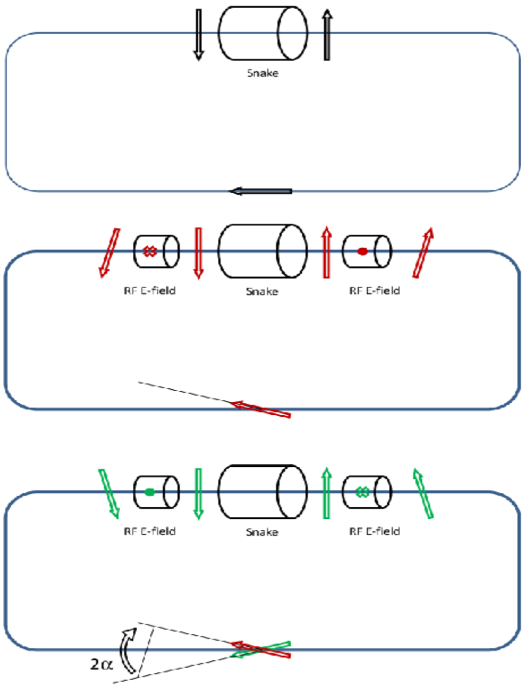

Figure 2.1: Concept of Siberian snake

For odd turns in the machine, an electric RF E-field perpendicular to the ring plane rotates the stable spin axis by a small angle α away from the longitudinal direction (middle panel). For even turns the RF E-field is reversed and the spin-closed orbit is then rotated by an angle of 2α. Since the angle is very small $\alpha \approx 10^{-7}$, the number of turns has to be very large ($n \approx 10^{10}$). With this settings one could reach an upper limit for the proton EDM of $d_p \approx 10^{-17} e \cdot cm$, which is rather limited but offers the opportunity for a first direct measurement of an proton EDM in a storage ring.

2.2.2 Orlov-Morse-Semertzidis Resonance Method

This method is based on using forced oscillations of particle velocities in resonance with the spin precession in order to expose the EDM ('resonance method') and alternately producing two sub-beams with different betatron tunes such that false EDM signals resulting from the ring imperfections could be corrected [16]. The idea is described by Orlov,Morse and Semertzidis. The concept describes the injection of sideways polarized particles into a machine with a vertical invariant spin axis. If one now oscillates the electric field $\vec{E}$ in the rest frame of the particle in resonance with the spin planar precession $\Omega_G = G\gamma\Omega_R$, one will observe a slow buildup of the vertical polarization of the particle proportional to the electric dipole moment. Ω_R denotes the revolution frequency $\Omega_R = \frac{2\pi\vec{v}}{L}$ of the polarized particle rotating in the storage ring. As shown in [16] the only way to produce this spin resonance with the help of such an electric field is to oscillate the particle lab frame velocity $\vec{v}$. The sensitivity for a proton EDM is estimated to reach $d_p = 10^{-29} \frac{e \cdot cm}{yr}$, but one have to challenge the problem of systematic errors.

2.2.3 Resonance EDM effect with RFE Flipper

This method focuses on a pure vertical ring magnetic field $\vec{B}$ and pure radial electric flipper field $\vec{E}$ with initial vertical particle spin. The radio-frequency electric flipper

RFE is installed in a section where the magnetic field vanishes $\vec{B} = 0$. If a charged particle passes through the RFE, the spin would precess for a non-vanishing EDM proportional to the electric field $\vec{E}$ in the RFE and the strength of the electric dipole moment $\vec{\Omega}_{EDM} = \eta \frac{q}{2m} \vec{E}$. For every particle pass through the RFE with the length L the initial vertical Spin $\vec{S} \| S_y$ is tilted and a longitudinal component occurs $S_z = S_y \cdot \alpha$ where $\alpha = \frac{\eta E L}{\beta}$. The so generated longitudinal spin would precess in the magnetic field of the ring with respect to the momentum vector with the frequency $f_s = \gamma G f_r$ where f_r denotes the ring frequency. Per single turn the angle of the spin precession is $\theta_s = 2\pi\gamma G$. The EDM effect on this frequency is very tiny, thus the precession will be not disturbed by that. If one now modulates the electric field in sync with the precession of the spin the EDM signal would build up.

2.2.4 Frozen Spin Method FSM

The idea of this method is to find the momentum of the particle where the spin precession and the momentum vector precess at the same rate thus the spin is kept along the momentum direction during the storage time as it is outlined in figure 2.2 (‘Frozen Spin‘) [17]. A radial electric field $\vec{E}$ in the rest frame on the particle acts on the EDM vector by precessing it out of plane and building up a vertical spin component. For a vanishing magnetic field $\vec{B} = 0$ and no parallel electric field components $\vec{\beta} \cdot \vec{E} = 0$ the spin precession rate with respect to the momentum vector precession rate is given by

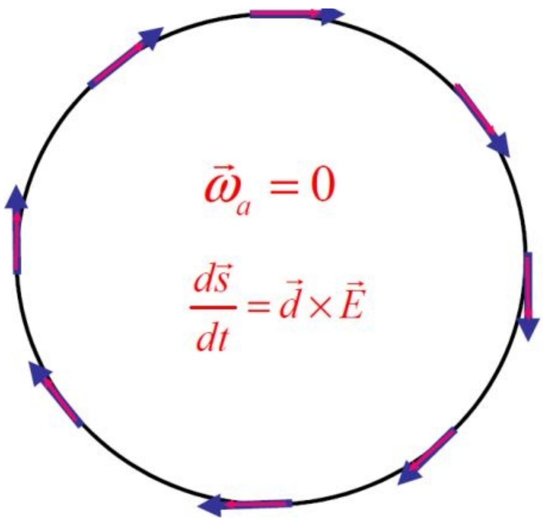

Figure 2.2: frozen spin method

$$\vec{\Omega}_a = \frac{q}{m} \left(\frac{1}{\gamma^2 - 1} - G \right) \vec{\beta} \times \vec{E} \tag{2.15}$$

The so called ‘magic‘ momentum locks the angle, i.e. $\Omega_a = 0$, as a function of time by setting:

$$\frac{1}{\gamma^2 - 1} - G = 0 \tag{2.16}$$

$$\rightarrow \gamma = \sqrt{\frac{1}{G} + 1} \tag{2.17}$$

This has only a real solution for $G > 0$, thus one can use the FSM in a ring with vanishing magnetic fields just for protons. One obtains a momentum for the proton of

$$p_p = \frac{m}{\sqrt{G}} = \frac{0.938\,\mathrm{GeV}}{\sqrt{1.79}} = 0.701\,\mathrm{GeV}. \tag{2.18}$$

For negative anomalous moments $G < 0$ one has to apply a combination of radial electric and dipole magnetic fields. The required E-field is given approximately by $E \approx GB\beta\gamma^2$. In the following table the required settings for a ring with a radius $r \approx 30$ are shown [13].

particle	p[GeV]	E $[\frac{MV}{m}]$	B[T]
proton	0.701	16.789	0
deuteron	1.000	-3.983	0.160
helium-3	1.285	17.158	-0.051

Since not all particles will be exactly at this "magic" momentum there is going to be a spread in the spin angles relative to their momentum vectors. In linear order this spread could be canceled by using an radio-frequency cavity in a straight section in the ring.

For the resonance and frozen spin method the spin coherence time SCT represents one of the limiting statistical factors. In the next chapter this quantity is discussed in more detail.

2.3 Spin Tune and Spin Coherence Time

The spin tune $\nu_s = \gamma G$ describes the number of spin oscillations per turn of the particle in the storage ring. It is proportional to the Lorentz γ-factor and the anomalous magnetic moment G of the particle. The spin coherence time τ_{SCT} denotes the time

Figure 2.3: Left panel: At injection all spin vectors are aligned and vertical polarized. Right panel: After some time, the spin vectors get out of phase and fully populate the cone, but the polarization is not affected

where the spin oscillations of a particle bunch remains in phase. A long τ_{SCT} is achieved when the spin tune among all particles remain approximatively the same. For different emittance and different momenta particles could have variant spin tunes and as consequence the spin oscillations becomes increasingly off-phase, i.e. the angle between the spin $\vec{s}_i$ vector and its corresponding invariant spin field vector $\vec{n}_i$ increases. For N particles the reciprocally spin coherence time denotes

$$\frac{1}{\tau_{SCT}} = \frac{1}{N}\sum_{j=1}^{N}\frac{1}{\vec{s}_j \cdot \vec{n}_j}\frac{d(\vec{s}_j \cdot \vec{n}_j)}{dt}. \tag{2.19}$$

For a vertical polarized beam the polarization is conserved even if the particles are out of phase (figure 2.3). If the particles are horizontally polarized the decoherence of the spins leads to an equally distributed spin orientation in the horizontal plane (see figure 2.4) and therefore the overall beam polarization decreases which aggravates the measurement of an EDM. For an experiment with a minimal detectable precession of

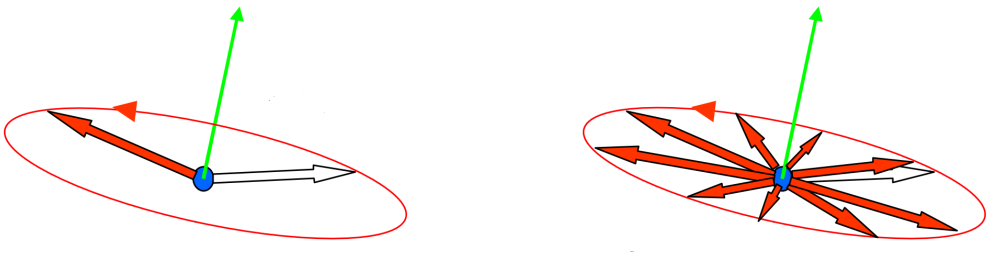

Figure 2.4: Left panel: At injection all spin vectors are aligned and horizontal polarized. Right panel: After some time, the spin vectors get out of phase and are fully distributed in the horizontal plane. The longitudinal polarization vanishes.

$\theta \approx 10^{-6}$ the storage time can be derived from

$$\theta_{EDM} = 2dEt \approx 5(10^{-9})\,\frac{\mathrm{rad}}{\mathrm{s}} \cdot 10^{-6}\,\mathrm{s} \approx \frac{10^{-15}\,\mathrm{rad}}{\mathrm{turn}}. \tag{2.20}$$

Assuming an EDM of $d \approx 10^{-29}\,\mathrm{e}\cdot\mathrm{cm}$ and an electric field of $E = 17\,\frac{\mathrm{MV}}{\mathrm{m}}$, approximately 10^9 turns are needed for a measurement of an deuteron EDM, which corresponds to a storage time of $t > 1000\,\mathrm{s}$. In chapter 4 the results of the beam time in May 2012 at COSY are discussed which was focused on increasing the SCT for varying conditions in the storage ring.

3 Polarimetry

In this section a short theoretical description of a polarization formalism is given, followed by an overview of polarimetry techniques and their implementations.

3.1 Formalism of Particle Polarization

The spin of a particle with spin $\frac{1}{2}$ can be described in quantum mechanical states by a Pauli spinor [18],

$$\chi = \begin{pmatrix} a_1 \\ a_2 \end{pmatrix} = a_1 \begin{pmatrix} 1 \\ 0 \end{pmatrix} + a_2 \begin{pmatrix} 0 \\ 1 \end{pmatrix} \tag{3.1}$$

where the amplitudes a_1 and a_2 are complex and $|a_1|^2 + |a_2|^2 = 1$. The expectation value of a spin operator A in the state χ is defined as,

$$\langle A \rangle = \langle \chi | A | \chi \rangle = \chi^\dagger A \chi \tag{3.2}$$

The corresponding operators for a spin $\frac{1}{2}$ particle are the Pauli matrices [19]

$$\sigma_x = \begin{pmatrix} 0 & 1 \\ 1 & 0 \end{pmatrix}, \sigma_y = \begin{pmatrix} 0 & -i \\ i & 0 \end{pmatrix}, \text{and } \sigma_z = \begin{pmatrix} 1 & 0 \\ 0 & -1 \end{pmatrix} \tag{3.3}$$

which yields to the spin three vector

$$\vec{S} = \frac{1}{2} \begin{pmatrix} \langle \sigma_x \rangle \\ \langle \sigma_y \rangle \\ \langle \sigma_z \rangle \end{pmatrix} = \frac{1}{2} \begin{pmatrix} a_1^* a_2 + a_2^* a_1 \\ -i a_1^* a_2 + i a_2^* a_1 \\ a_1^* a_2 + a_2^* a_1 \end{pmatrix} \tag{3.4}$$

This spin three vector can be treated as a classical vector in case of spin precession. For an ensemble of N particles a set of Pauli spinors can be defined by,

$$\chi^{(n)} = \begin{pmatrix} a_1^{(n)} \\ a_2^{(n)} \end{pmatrix} \tag{3.5}$$

where n runs from 1 to N counting all involved particles. For averaging the spin a beam spin can be described through the density matrix:

$$\rho = \frac{1}{N} \begin{pmatrix} \sum_{n=1}^{N} |a_1^{(n)}|^2 & \sum_{n=1}^{N} a_1^{(n)} a_2^{(n)*} \\ \sum_{n=1}^{N} a_2^{(n)} a_1^{(n)*} & \sum_{n=1}^{N} |a_2^{(n)}|^2 \end{pmatrix}, \tag{3.6}$$

This matrix represents the direction and the magnitude of the spin expectation of the particle beam and can be expanded into a combination of Pauli spin operators

$$\rho = \frac{1}{2}\left(I + \sum_{j=x,y,z}^{3} p_j \sigma_j\right) \tag{3.7}$$

where I is the unit matrix

$$I = \begin{pmatrix} 1 & 0 \\ 0 & 1 \end{pmatrix}. \tag{3.8}$$

The p_j coefficients represent the spatial components in the x,y and z directions of a chosen coordinate system. The vector

$$\vec{p} = \begin{pmatrix} p_x \\ p_y \\ p_z \end{pmatrix}. \tag{3.9}$$

can be interpreted as a classical vector representing the polarization of the beam. For spin 1 particles like deuterons the formalism works in analogy with the spin $\frac{1}{2}$ ones. The difference is that now the spin can have three states: -1, 0 and 1. In consequence the spinor of the particle has to have three components

$$\chi = \begin{pmatrix} a_1 \\ a_2 \\ a_3 \end{pmatrix}. \tag{3.10}$$

The basic angular momentum operators for a spin 1 particle are

$$S_x = \frac{1}{\sqrt{2}}\begin{pmatrix} 0 & 1 & 0 \\ 1 & 0 & 1 \\ 0 & 1 & 0 \end{pmatrix}, S_y = \frac{1}{\sqrt{2}}\begin{pmatrix} 0 & -i & 0 \\ i & 0 & i \\ 0 & i & 0 \end{pmatrix}, \text{and}\, S_z = \frac{1}{\sqrt{2}}\begin{pmatrix} 1 & 0 & 0 \\ 0 & 0 & 0 \\ 0 & 0 & -1 \end{pmatrix} \tag{3.11}$$

These operators including the 3×3 identity matrix are not sufficient to describe the state of a spin 1 particle completely. Five other Hermitian operators are still necessary.

A tensor of rank two can be constructed from nine operator products of the spin component operators S_x, S_y and S_z.

$$T = \begin{pmatrix} S_x \\ S_y \\ S_z \end{pmatrix}\begin{pmatrix} S_x & S_y & S_z \end{pmatrix} = \begin{pmatrix} S_xS_x & S_xS_y & S_xS_z \\ S_yS_x & S_yS_y & S_yS_z \\ S_zS_x & S_zS_y & S_zS_z \end{pmatrix} \tag{3.12}$$

In standard Cartesian notation a set of ten operator can be constructed:

$$I = \begin{pmatrix} 1 & 0 & 0 \\ 0 & 1 & 0 \\ 0 & 0 & 1 \end{pmatrix}$$

$$S_x;\ S_y;\ S_z$$

$$T_{xy} = 3S_xS_y; T_{xy} = 3S_xS_z;\ T_{yz} = 3S_yS_z;$$

$$T_{xx} = 3S_xS_x - 2I;\ T_{yy} = 3S_yS_y - 2I;\ T_{zz} = 3S_zS_z - 2I;$$

From these ten operators only nine can be independent. Considering the relation

$$Txx + Tyy + Tzz = \begin{pmatrix} 0 & 0 & 0 \\ 0 & 0 & 0 \\ 0 & 0 & 0 \end{pmatrix}$$

one can replace one operator by a pair of the other two which yields in a complete set of orthogonal operators. The density matrix of an ensemble for spin 1 particles can now be written as

$$\rho = \frac{1}{3}\left(I + \sum_i p_iS_i + \sum_{i,j} p_{ij}T_{ij}\right) \tag{3.13}$$

where p_i and p_{ij} stand for the polarizations associated with each operator.
Typical polarized beam sources that may be used for the deuteron EDM search posses axial symmetry. In that case all off diagonal elements of ρ are zero. Assuming the z axis as the symmetry axis equation 3.13 can be simplified to

$$\rho = \frac{1}{3}\left(I + p_zS_z + \frac{1}{2}p_{zz}T_{zz}\right) \tag{3.14}$$

One can now identify the vector polarization P_V and tensor polarization P_T by the population densities,

$$P_V = p_z = \frac{\rho^+ - \rho^-}{\rho^+ + \rho^0 + \rho^-} \tag{3.15}$$

$$P_T = p_{zz} = \frac{\rho^+ + \rho^- - 2\rho^0}{\rho^+ + \rho^0 + \rho^-}, \tag{3.16}$$

where $\rho^+ = \sum |a_1^{(n)}|$, $\rho^0 = \sum |a_2^{(n)}|$, and $\rho^- = \sum |a_3^{(n)}|$.

3.2 EDDA Polarimeter at COSY

Assuming an EDM experiment where the spin is slowly build up from the longitudinal polarization to the vertical direction, one has to sample small changes of the vertical component ($\approx 10^{-6}$ per turn). This requires a high sensitivity and a large analyzing power of the polarimeter and one has to keep the systematic errors below the signal level. For these requirements the EDDA system located on the Cooler Synchrotron (COSY) at Jülich was chosen to study systematics and properties of the polarimeter and the storage ring. The EDDA detector was originally

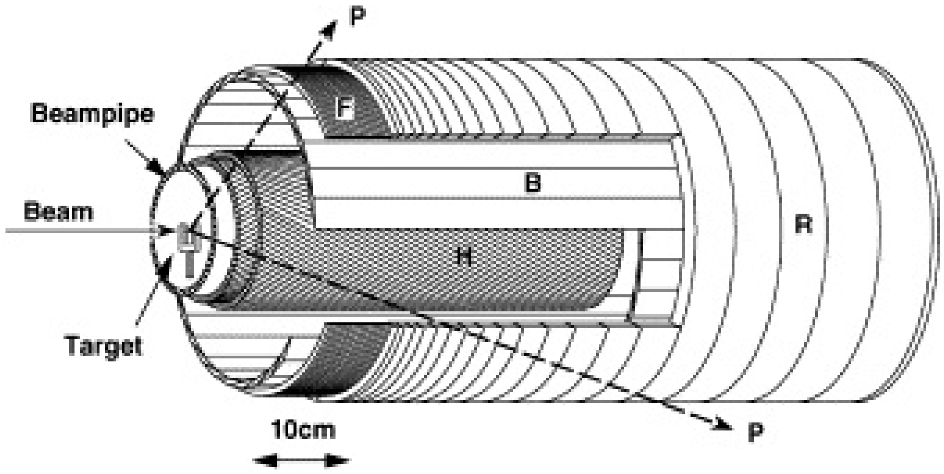

Figure 3.1: Scheme of the EDDA detector: Internal Cosy beam, beampipe (160mm diameter, 2mm thick Aluminum tube), inner detector shell with scintillating fibers H, outer detector shell with scintillator bars B, scintillator semirings R and semirings from scintillating fibers F

designed for measurements of proton-proton elastic scattering excitation functions for energies from 0.5 to 2.5 GeV [20]. In figure 3.1 a schematic view of EDDA is shown.

The detector consists of several ring and bar scintillators for the measurements of ϕ and θ in an arrangement that wraps completely around the beampipe downstream of the target position. For the first high efficient investigations of the detector systematics a thick carbon target was chosen 3.2. The beam of polarized deuterons was slowly extracted by moving it into the target direction. The advantage of choosing polarized deuterons is the well-known and easy method to polarize them and that they can simply be measured by an elastic scattering on the carbon target. The sensitivity and efficiency of a polarimeter like EDDA is discussed in the following

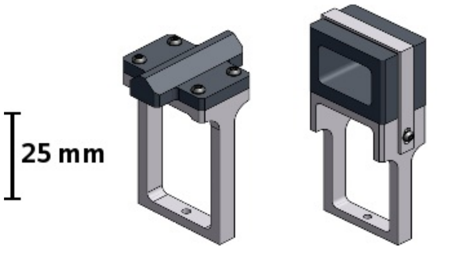

Figure 3.2: Carbon target of EDDA

section. Before discussing the sensitivity one has to define the signal of the elastic scattering.

3.2.1 Signal

The differential elastic cross section for a polarized deuteron (spin 1 particle) interacting with an unpolarized target is given by [19]

$$
\begin{aligned}
\frac{d\sigma}{d\Omega}(\theta,\phi,\beta) = \frac{d\sigma_{unp}}{d\Omega}(\theta)[(1{+}2\frac{\sqrt{3}}{2}P_V \sin\beta \sin\phi \; iT_{11}(\theta) \\
+\frac{1}{2\sqrt{2}}P_T(3\cos^2\beta - 1)T_{20}(\theta) \\
-2\sqrt{\frac{3}{2}}P_T \sin\beta\cos\beta\cos\phi \; T_{21}(\theta) \\
+2\frac{\sqrt{3}}{4}P_T\sin^2\beta\sin 2\phi \; iT_{22}(\theta)],
\end{aligned}
$$

where P_V and P_T are the vector respectively tensor polarization (see 3.15 and 3.16) and further iT_{11} and T_{2m} stand for the corresponding analyzing powers. $\frac{d\sigma_{unp}}{d\Omega}$ denotes the differential cross section for unpolarized scattering. For a purely vector polarized beam with I particles per second impinging on a target of thin thickness and a density ρ, the counting $N^{(i)}$ rate of a detector element i with solid angle $\Omega^{(i)}$ is given by

$$
\begin{aligned}
N^{(i)} &= I\rho\int_{\Omega^{(i)}}\frac{d\sigma}{d\Omega}(\theta,\phi,\beta)\,d\Omega & (3.17)\\
&= I\rho\int_{\Omega^{(i)}}\frac{d\sigma_{unp}}{d\Omega}(\theta)d\Omega + \sqrt{3}P_V\sin\beta\int_{\Omega^{(i)}}\left[\frac{d\sigma_{unp}}{d\Omega}(\theta)iT_{11}(\theta)\sin\phi\right]d\Omega & (3.18)\\
&= N_0^{(i)}\left[1+\sqrt{3}P_V\sin\beta A_0^{(i)}\right], & (3.19)
\end{aligned}
$$

with the variables $N_0^{(i)}$ and $A_0^{(i)}$ defined as

$$
\begin{aligned}
N_0^{(i)} &= I\rho\int_{\Omega^{(i)}}\frac{d\sigma_{unp}}{d\Omega}(\theta)\sin\theta d\theta d\phi, & (3.20)\\
A_0^{(i)} &= \frac{1}{N_0}\int_{\Omega^{(i)}}\left[\frac{d\sigma_{unp}}{d\Omega}(\theta)i_{11}(\theta)\sin\phi\right]\sin\theta d\theta d\phi. & (3.21)
\end{aligned}
$$

The rates for two similar detectors at identical scattering angle θ centered at $\phi_1 = -\frac{\pi}{2}$ and $\phi_2 = \frac{\pi}{2}$, i.e. left and right of the beam, will be affected in a different way. One gets $\sin\phi_1 = -1$ and $\sin\phi_2 = 1$, so for the counting rates

$$
\begin{aligned}
N(\phi_1 = -\frac{\pi}{2}) &= N_0\left[1-\sqrt{3}P_V\sin\beta A_0\right], & (3.22)\\
N(\phi_2 = \frac{\pi}{2}) &= N_0\left[1+\sqrt{3}P_V\sin\beta A_0\right]. & (3.23)
\end{aligned}
$$

The relative asymmetry $\mathcal{A}$ of these rates is a measure of P_V and A_0

$$\mathcal{A} = \frac{N(\frac{\pi}{2}) - N(-\frac{\pi}{2})}{N(\frac{\pi}{2}) + N(-\frac{\pi}{2})} = \sqrt{3} P_V A_0 \sin \beta, \tag{3.24}$$

i.e. one can determine the vector polarization P_V of a particle beam when A_0 is known

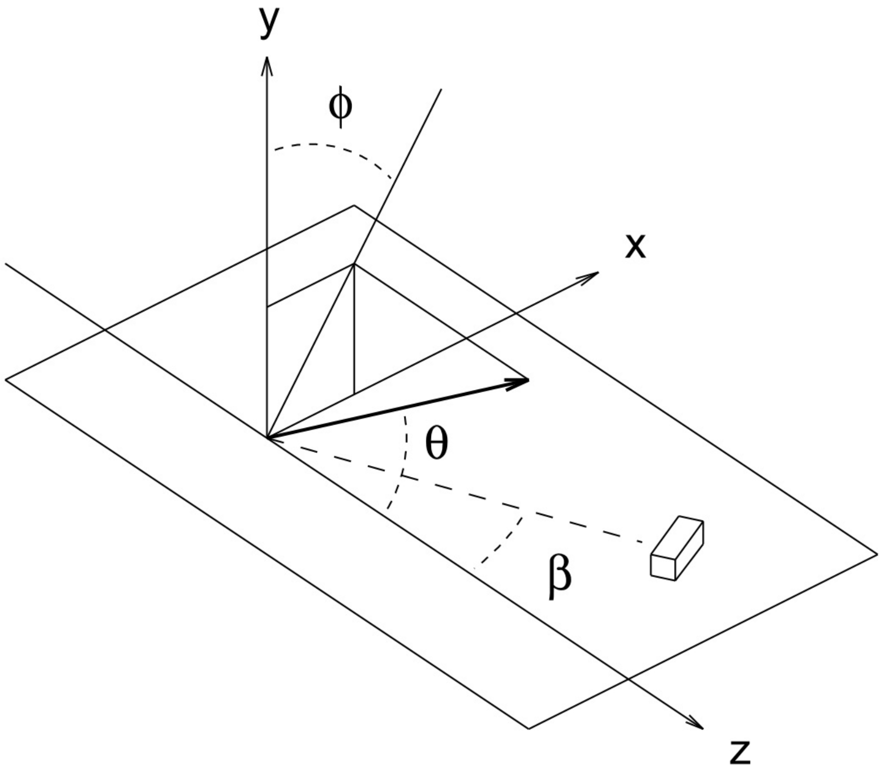

Figure 3.3: The coordinate system for polarization direction (arrow) based on the observation of the reaction product in a detector(small box). The beam travels along the z-axis. The detector position at an angle β defines the reaction plane and positive x. The quantization axis for the polarization lies in a direction given by the polar angle θ and ϕ as measured from the y axis.

without knowing the particle flux I. The laboratory frame has not to be necessarily the same as the scattering frame. Usually the z-axis is defined as the beam momentum axis. The orientation of the spin, which defines the y axis in the scattering frame, then defines a rotation about the z-axis of the scattering plane with respect to the laboratory frame (figure 3.3). The azimuthal angle ϕ of a detector in the laboratory frame is then shifted by $\Delta\phi$ compared to the corresponding angle in the scattering plane. $\Delta\phi$ is the enclosed angle between the spin plane and the laboratory y-z plane.

By rotating the plane of figure 3.3 about the z axis the detectors can be placed at x($\phi = \pi$) and -x($\phi = 0$). In the laboratory frame this setting is sensitive to the vertical component of the vector polarization P_V and its associated analyzing power $\mathcal{A}_{LR}$

$$\mathcal{A}_{LR} = \frac{L-R}{L+R} = P_V A_0 \sin\beta \cos\Delta\phi = P_V^y A_0 = \epsilon_{LR} \quad \rightarrow \quad P_V^y = \frac{\mathcal{A}_{LR}}{A_0}. \tag{3.25}$$

With L respectively R represent the rate in the left and right detector. During the storage time of the deuterons the size of P_V^y will uniformly increase proportional to the EDM.

For a horizontal polarized beam the measurement method works equally with a detector pair placed above and below the beam ($\phi = -\frac{\pi}{2}$ and $\phi = \frac{\pi}{2}$). The ratio $\mathcal{A}_{DU}$ is then given by

$$\mathcal{A}_{DU} = \frac{D-U}{D+U} = \sqrt{3} P_V A_0 \sin\beta \cos\Delta\phi = P_V^x A_0 = \epsilon_{DU} \quad \rightarrow \quad P_V^x = \frac{\mathcal{A}_{DU}}{A_0}. \tag{3.26}$$

where D and U stand for the rates in the "down" and "up" detector, respectively.

3.2.2 Efficiency

The efficiency of a polarimeter is defined as the ratio between the number of scattered particles used for polarimetry and the number of particle stored in the experiment. For a single detector element i it can be calculated by

$$\eta^{(i)} = \frac{N_0^{(i)}}{I} = \rho \int_{\Omega^{(i)}} \left(\frac{d\sigma}{d\Omega^{(i)}} \right) d\Omega. \tag{3.27}$$

The statistical uncertainty of the asymmetry can be evolved by the propagation of error as

$$\sigma^2_{A_{LR}} = 4 \frac{L^2 \sigma_R^2 + R^2 \sigma_L^2}{(L+R)^4} = 4 \frac{LR}{(L+R)^3}. \tag{3.28}$$

Using the known rates this can be written as

$$\sigma^2_{A_{LR}} = 4 \frac{N_0^2 \left[1 - 3(P_V^y)^2 A_0^2\right]}{8 N_0^3} \approx \frac{1}{2N_0}, \tag{3.29}$$

for small values of $3(P_V^y)^2 A_0^2$ as it will be in an EDM experiment with deuterons. One can now calculate the error of P_V^y as

$$\sigma^2_{P_V^y} = \frac{\sigma^2_{A_{LR}}}{A_0^2} = \frac{1}{2 N_0 A_0^2}. \tag{3.30}$$

The dominator of this term is referred to as the figure-of-merit depending on the scattering cross section and the detector acceptance A_0.

$$\mathrm{FOM}(\theta) = \sigma_{unp}(\theta) A_0(\theta)^2 \tag{3.31}$$

Providing a good statistical basis for the measurement the challenge is to find the best balance between the large cross section at small angles and the large analyzing powers at large angles. In the next chapter the results of the beam time at COSY in May 2012 are discussed.

4 Data Analysis of the Beam Time at COSY (May 2012)

As described in 2.3 the spin coherence time SCT plays a crucial role in the measurement of a potential EDM. Therefore one goal of the May 2012 beamtime at COSY was to improve the understanding of the SCT. To study the feasibility of optimizing the SCT at COSY a bunched beam of horizontal polarized deuterons was stored in the ring and slowly drifted to a carbon target, so that elastic scattering between deuterons and the carbon nucleons takes place. The kinetic energy of the deuterons is about $E_{kin} = 232\,\mathrm{MeV}$, which leads to a beam momentum of $p = 0.97\,\mathrm{GeV}$. In this chapter the techniques and the results of this experiment are presented and discussed.

4.1 Implementation of the Experiment

One important requirement to measure a proton, deuteron or light nuclei EDM is a high sensitive polarimeter with a very good efficiency. The key to efficient polarimetry is to interact the beam with a thick target by elastic scattering. Therefore a tube target made of carbon was designed and placed in front of the detector. Due to the geometric limitation of the detector system one is limited to a target thickness of 1.5 cm with an opening of 2.5 cm (see figure 3.2). Slow extraction of the stored deuteron beam by shifting it into the target, yields to an effective analyzing power of $\frac{3A_y}{2} = 0.67(4)$ and an efficiency near $\eta = 10^{-3}$, i.e. for every 1000 particles extracted from the beam, one should be scattered from the target material and recorded for polarization calculation. In addition one has to monitor any systematic errors arising from geometric or counting rate changes during the beam store. These requirements were met in a first study in 2009 with polarized deuterons at COSY. A summary of these investigations is given in the article [21] by Ed Stephenson.

The EDM signal is the rotation of the polarization from its initial direction parallel to the velocity. Only the vertical polarization component is stable in a storage ring thus the polarization will precess in the horizontal plane at a high rate determined by the spin tune $\nu_S = \gamma G$. The momentum spread of the beam will quickly decohere the longitudinal polarization. This first-order problem is solved by bunching the beam, thus all orbit periods should be the same on average. However, emittance and small non-linear momentum effects will lead to different path length, changes to γ, and a spread in the spin tunes of the particles in the bunch. Including beam cooling (electron-beam or stochastic) will reduce the emittance and momentum spread. In addition, sextupole fields or even higher order fields could correct the orbit lengths of the particles. Since the deuterons are initially injected in the ring with a vertical polarization, a radio frequency RF solenoid is used to rotate the spin of the particles into the horizontal plane. To measure the spin coherence time of the particles, the asymmetry and, thus, the polarization of the beam has to be determined as a function of time. In the following section the DAQ and the time stamp analysis to extract the horizontal polarization are discussed.

4.1.1 Data Handling

The data of a turn are taken by starting with a vertically polarized beam, which is rotated into the horizontal by means of a RF solenoid. Pre-scaled signals from the RF signals for the solenoid as well as for COSY are put on time-to-digital-converter TDC. In addition, a signal is provided as soon as both signals are once in the same phase.

4.1.1.1 Data Format

The precision of the time stamps from the TDC and the system controller is 92.59 ps with a full range of 6.4 μs. The precision, respectively the bin width can be adjusted during the set up by using a control parameter hs_{div} setting the bin width to $bw = \frac{25\,\mathrm{ns} \cdot 128}{216 \cdot hs_{div}}$. For the DAQ the parameter was set to $hs_{div} = 160$. Each overflow of this full range is counted internally up to a maximum range of about 6.7 s (20 bit) for the TDC and 0.21 s (15 bit) for the system controller, whereas both systems run synchronized. For time measurements beyond this maximum range the corresponding offsets have to be counted within the data analysis, thus the signals on the TDC have to be more frequent than once per 6.7 s and the read out trigger for the DAQ has to come at least every 0.21 s. With this method one provides a precise time stamp for every signal since start of the run.

The data are divided in two different data streams within the DAQ using two different sequences of event numbers. The TDC readout is asynchronously, i.e. whenever data are available the system controller reads out these data and send them to the attached readout computer. In addition, whenever a read-out trigger occurs, the system controller reads out the complete crate including the TDC and sends the data to the attached computer, as well. The latter event stream contains a time stamp from the system controller and is synchronized with the rest of the DAQ. Before the data are analyzed, both data streams are merged together by assigning all asynchronous data to the next synchronized event.

4.1.1.2 Time Stamping

For defining the macroscopic time three definitions are used:

- The start of a cycle is defined as the point in time when the polarization bits change from 0 to a defined value.
- The start of the analysis period is defined as the point in time when the flat top bits change from 0 to 1. This is used for the analysis of the vertical polarization.
- The horizontal polarization can only be extracted once the phase-match time stamp between two RFs signals has appeared. Thus, the starting time $t = 0$ for the horizontal analysis is defined. For the current period, this time stamp appeared about 6.35 s after the flat top signal.

A usual run consists in general of about 57 cycles, where every cycle lasts for 120 s. There are three polarization states: two vector polarized $P_V = -1, +1$ and one tensor polarized beam $P_T = 0$, thus every third cycle is of the same polarization state. The variable $P_{V,T}$ does not describe the real polarization but stands for initial polarization state at the beginning of a cycle.

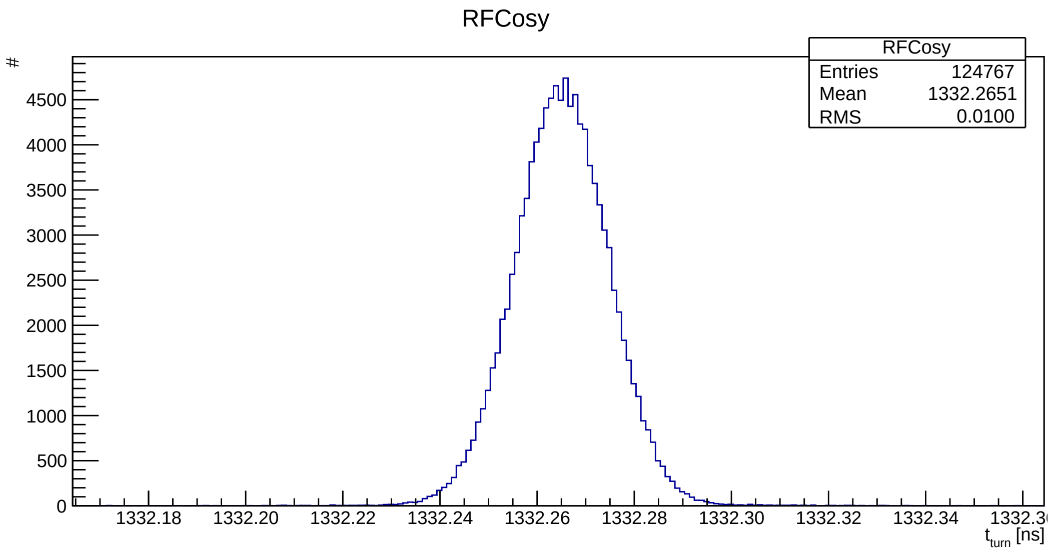

Figure 4.1: Time distribution T_{RFCosy} of the RF COSY signal

The pre-scaled signal from the RF solenoid is used to time-stamp and count the number of turns. For this, the difference between two signals $T_{RF,i+1}$ and $T_{RF,i}$ is divided by the pre-scale factor n_{ps} and the result is used to get the interpolated time stamps for the turns in between:

$$T_{turn} = \frac{T_{RF,i+1} - T_{RF,i}}{n_{ps}} = \frac{T_{RFCosy}}{n_{ps}} \tag{4.1}$$

and

$$T_{RF,i,j} = T_{RF,i} + j \cdot T_{turn}, \quad j = 0...n_{ps} - 1, \tag{4.2}$$

where $T_{RF,i,j}$ denotes the time of the j^{th} turn after $T_{RF,j}$.

The time of one beam turn T_{RFCosy} is monitored and saved in a histogram. In figure 4.1 an exemplary distribution of the COSY period T_{RFCosy} in nanoseconds is shown. The frequency f_{RFCosy} of the beam stored in the ring is calculated by

$$f_{RFCosy} = \frac{1}{T_{RFCosy}} = \frac{1}{1332.2651\,\text{ns}} \approx 750.601\,\text{kHz} \tag{4.3}$$

The time stamps for the pre-scaled RF solenoid signal are determined in the same way as the COSY RF period. The measured time $T_{RFSolenoid}$ is also saved in a histogram, which is plotted in figure 4.2.

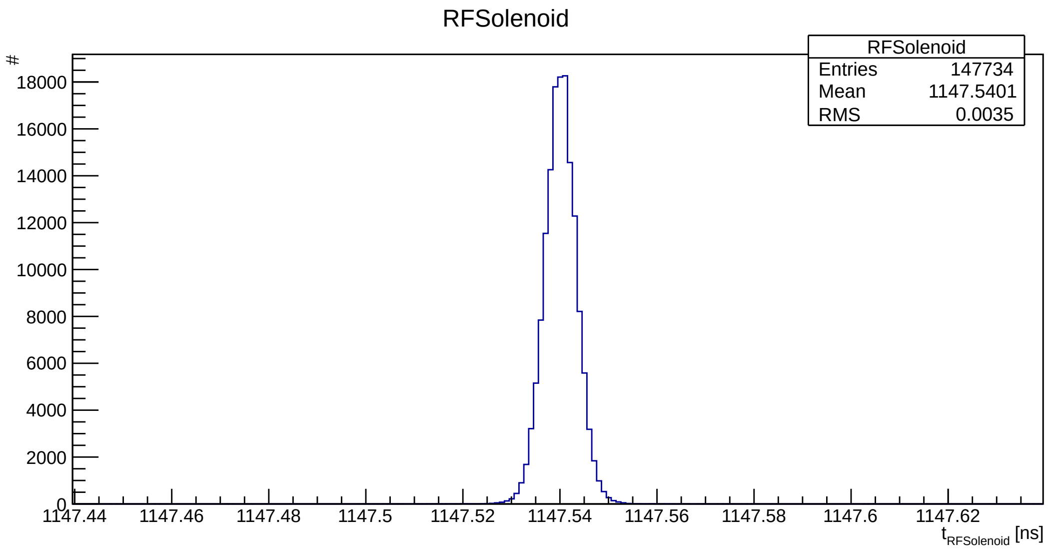

Figure 4.2: Time distribution $T_{RFSolenoid}$ of the RF soneloid signal

In this case one gets for the frequency of the solenoid:

$$f_{RFSolenoid} = \frac{1}{T_{RFSolenoid}} = \frac{1}{1147.5401\,\text{ns}} \approx 871.429\,\text{kHz} \tag{4.4}$$

Knowing the time stamp for each turn of the beam T_{turn}, the relative time of every polarimeter signal can be extracted, which corresponding to a position within that turn

$$t_{signal,rel} = t_{signal} - t_{RF,i,j}, \tag{4.5}$$

with $t_{RF,i,j}$ being the last interpolated RF time stamp before the signal itself. Fig 4.3 shows a plot of the signal time distribution within a turn as function of the macroscopic cycle time.

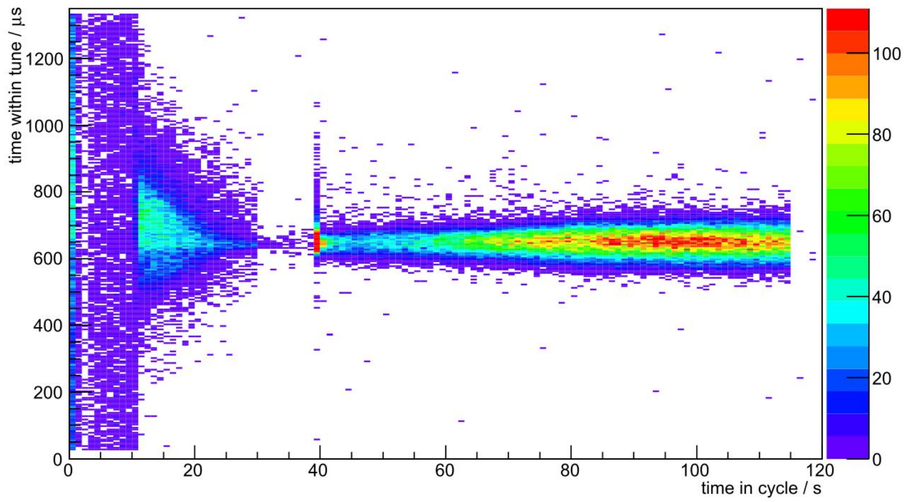

Figure 4.3: Signal time distribution within a turn as function of the macroscopic cycle time

In figure 4.3 one can see the slow movement of the beam into the target. It is demonstrated, that at the beginning of the horizontal polarization measurement ($t = 40\,\mathrm{s}$) the number of the scattered deuterons is small and is increasing constantly until the center of the beam is reached. This is explainable by a spherical beam geometry, where less particles are located at the edges of the beam profile. If the center of the beam is moved closer to the target, the rate of scattered deuterons will increase.

4.1.2 RF Solenoid

As mentioned before the RF solenoid (figure 4.4) was used to shift the initial vertical polarization of the beam into the horizontal plane. The ramp up and ramp down time of the solenoid is about 200 ms. In fig 4.5 the effect of the solenoid on the vertical polarization is shown. The y-axis represents the left-right asymmetry in the counting rates of the detector, which corresponds directly to a measurement of the vertical polarization. The fol-

Figure 4.4: Picture of the RF solenoid operating in COSY on the spin tune resonance

lowing steps are identifiable in the plot:

- At the beginning of the run the solenoid is turned off and the left-right asymmetry stays constant. The negative asymmetry denotes a polarization state $P_V = -1$.
- After about 6.35 s to 13 s the solenoid is activated and the vertical polarization starts to oscillate. The period is proportional to the strength of the solenoid.
- Then the solenoid is turned off when the vertical polarization vanishes and the spin is precessing in the horizontal plane, thus there is no variation of the asymmetry.
- At $t_{cycle} \approx 64$ s the solenoid is turned on again and the polarization is rotating in the vertical plane.

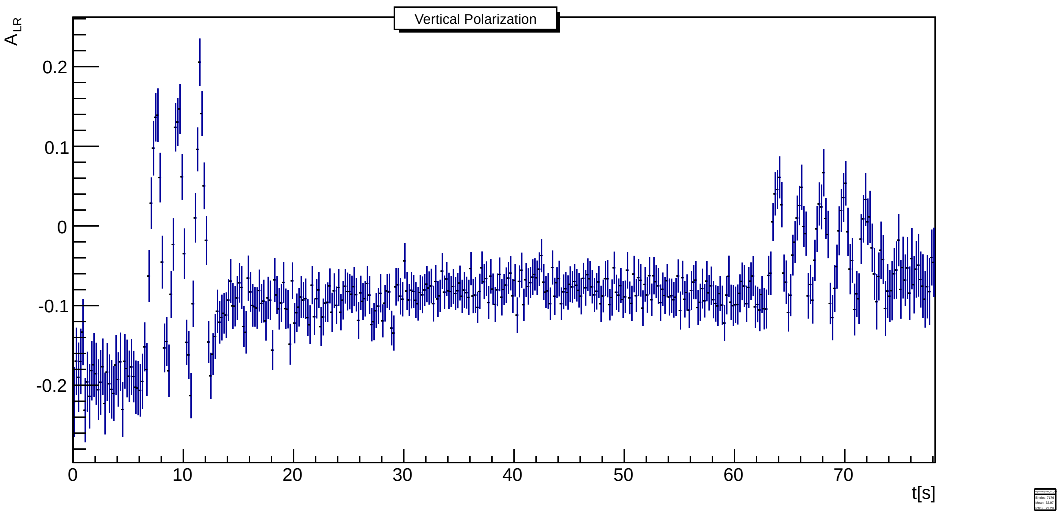

Figure 4.5: Example of the a vertical polarization measurement

The RF solenoid is operating at the first negative harmonic (H=-1) of the spin tune frequency

$$f_{RFSolenoid} = (1 - \gamma G) \cdot f_{RFCosy} = (1 - \nu_S) \cdot f_{RFCosy}, \tag{4.6}$$

where $2\pi \cdot \gamma G$ describes the angle between the beam momentum and the spin after one turn in the storage ring. This choice was made to put the frequency in a good operating range for the solenoid power range. In addition, the spin tune frequency f_{ν_S} can be measured by matching it with the RF solenoid system. Only when both are on the resonance better than 1Hz the oscillation continue with no deterioration of the amplitude. In the next section the investigation of the vertical polarization for various runs is presented.

4.2 Analysis of the Vertical Polarization

In this section the vertical polarization of the beam is discussed for 60 runs. The left-right asymmetry is calculated by the following equation

$$\mathcal{A}_{LR} = \frac{L - R}{L + R} = \epsilon_{LR}, \tag{4.7}$$

where L and R represents the counting rates in the left and right detector respectively. The error of the asymmetry is calculated by

$$\sigma_{\mathcal{A}_{LR}} = \frac{2(R\sigma_L + L\sigma_R)}{(L + R)^2}, \tag{4.8}$$

with $\sigma_L = \sqrt{L}$ and $\sigma_R = \sqrt{R}$.

To analyze the left-right asymmetry the distribution in figure 4.5 was fitted by two sine curves, one for the first and one for the second oscillation respectively, and three constant terms before, between and after the oscillations. In figure 4.6 an example of a fitted distribution is shown taking into account the continuity at the transitions. The fit data comprises the offset, the amplitude and the period of the first oscillation.

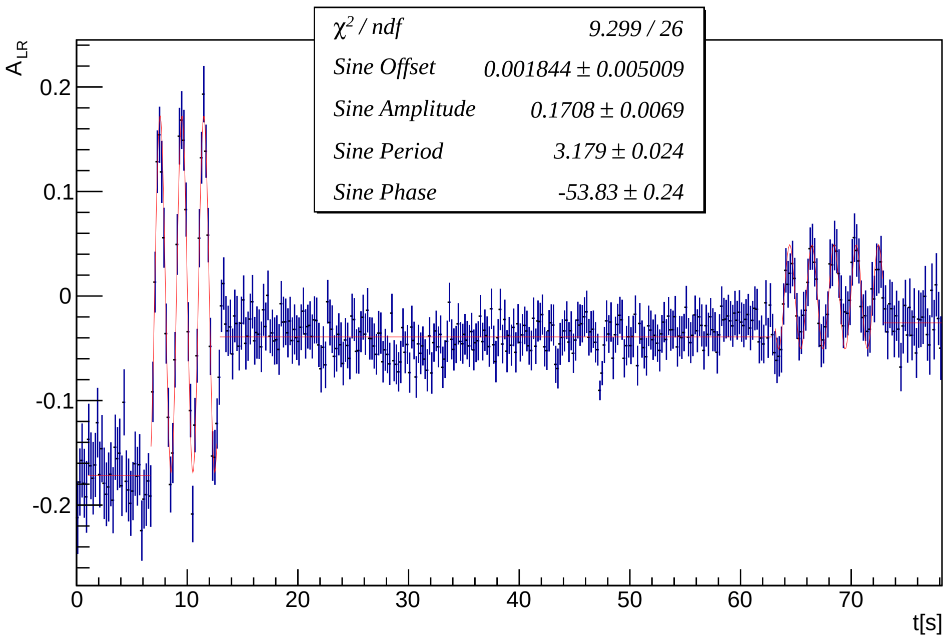

Figure 4.6: Vertical polarization fitted by sine curves for polarization state $P_V = -1$

First of all the times of turning on and off the solenoid are discussed. Defining t_1 and t_2 as the starting and ending point of the first oscillation, t_3 and t_4 describes it

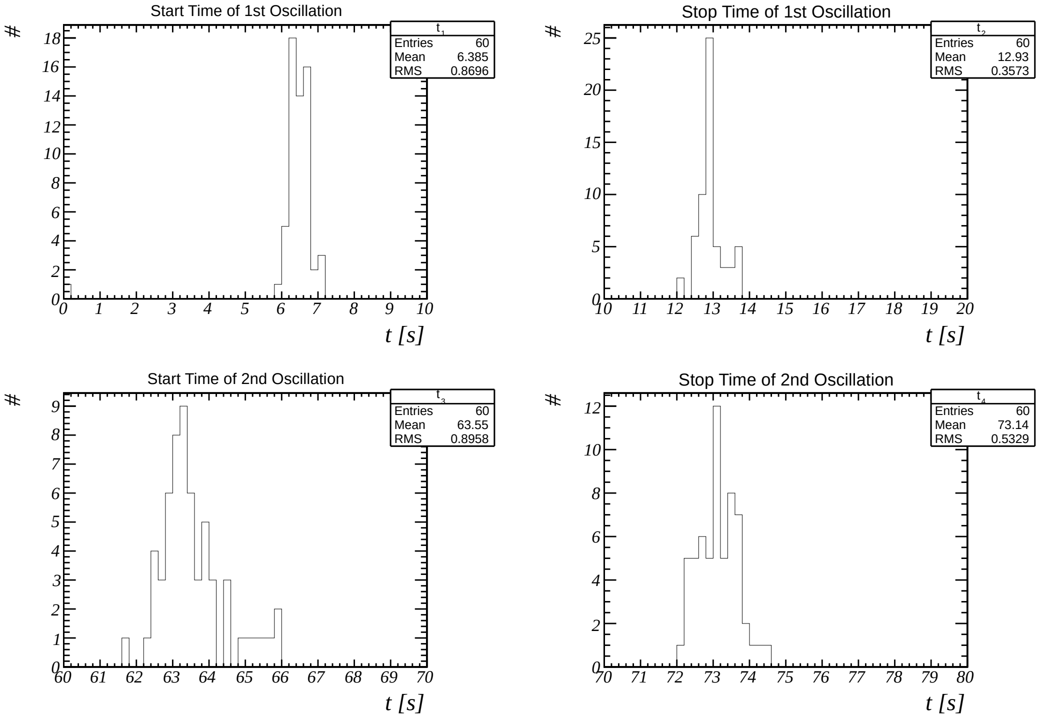

Figure 4.7: Time distribution for polarization state 01: $P_V = -1$

for the second oscillation respectively. In 4.7 the distribution of these values for the polarization state $P_V = -1$ are plotted.

It is obvious that all values are close to each other, which is strengthen by the small RMS of the distributions. In table 4.1 the mean and the RMS of both polarization states are given. One can see, that all time values are compatible with each other

	$t_1[s]$	$t_2[s]$	$t_3[s]$	$t_4[s]$
$P_V = 1$	6.405±0.893	12.94±0.38	63.42±0.93	73.34±0.64
$P_V = -1$	6.385±0.870	12.93±0.36	63.55±0.90	73.14±0.54

Table 4.1: Table of the starting and ending times of the sine oscillations

within their errors. This indicates, that the solenoid was always used at the same times in the cycles.

Another interesting quantity is the strength of the solenoid and its stability in time. The strength of the solenoid is defined as the number of vertical polarization oscillations during one beam turn

$$\epsilon = \frac{T_{COSY}}{T_{P_V}} \approx 10^{-7}, \tag{4.9}$$

where T_{P_V} denotes the period time of one oscillation of the vertical polarization. This leads to an integrated B-field of the solenoid of

$$\int B \cdot dl = \frac{4\pi\epsilon B\rho}{1+G} \approx 200\,\mathrm{G}\cdot\mathrm{cm}, \tag{4.10}$$

where $B\rho$ is the rigidity of the storage ring. One sees that the period of the oscillation of the polarization T_{P_V} in the vertical plane is inverse proportional to the strength of the solenoid, thus one has to compare the first and second period length in one cycle and furthermore one has to check, if the period stays constant for all runs. The

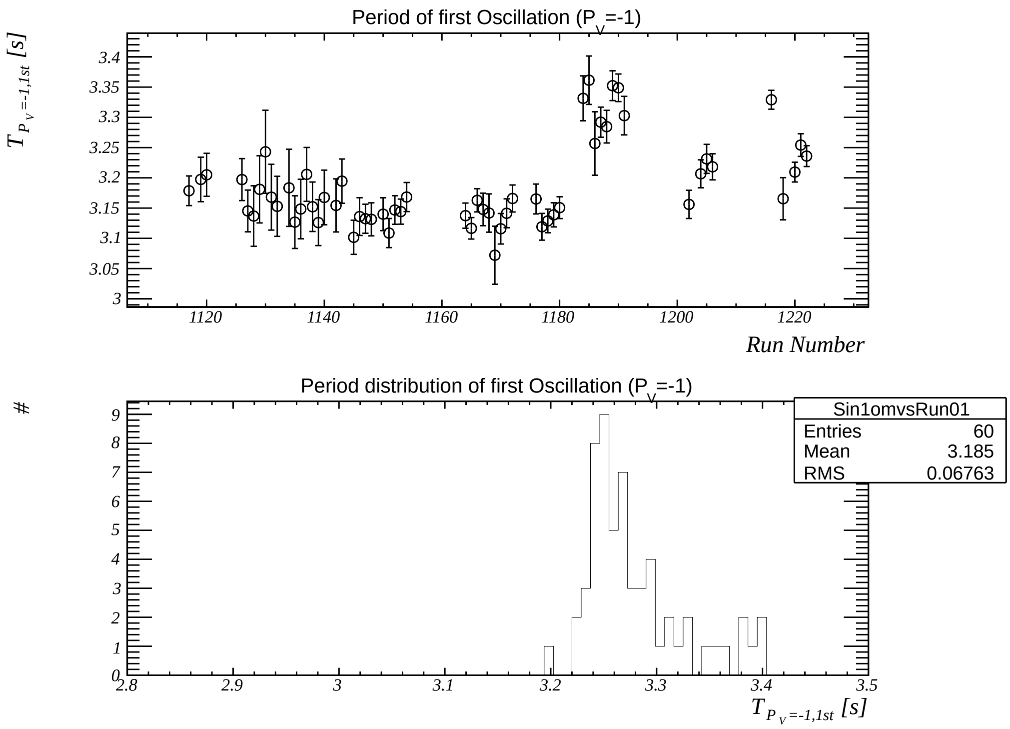

Figure 4.8: Upper panel: The period of the first oscillation is plotted against the runs. Lower panel: The distribution of these periods is shown.

letter purpose is handled in figure 4.8, where in the upper panel the periods of the first oscillation in polarization state $P_V = -1$ are plotted against the runs. The lower panel of the figure shows, that the period do not change significantly, thus one can assume a constant solenoid strength over the time.

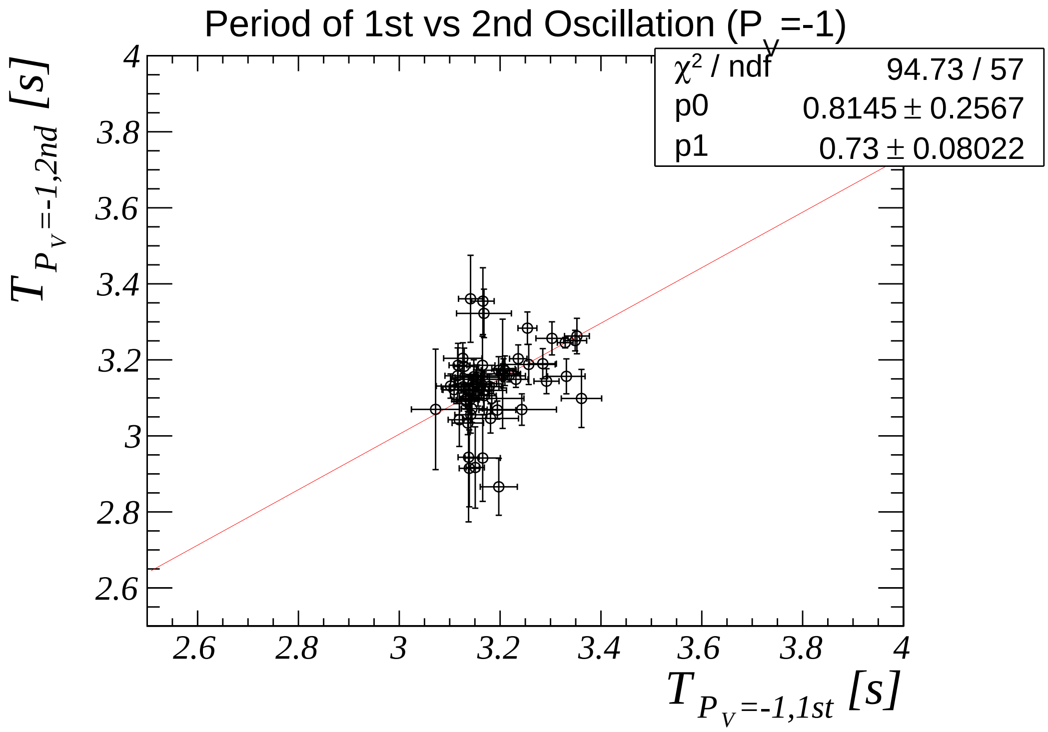

Figure 4.9: Period of the second $T_{P_V=-1,2nd}$ versus the first oscillation $T_{P_V=-1,1st}$ for polarization state $P_V = -1$

In figure 4.9 the periods of the first oscillation are plotted against the periods of the second one. As previously, this plot represents the data from measurements of the polarization state -1. One recognizes that the entries are concentrated in one point, thus the period stays constant over one cycle, which indicates a stable solenoid strength, as well.

An additional quantity which can be studied is the initial vertical polarization of the beam. Therefore the first constant term of the left-right asymmetry distribution in figure 4.6 has to be examined. In figure 4.10 the values of the initial left-right asymmetry is plotted versus the run. One sees, that the polarization is nearly the same for all runs and within their errors. This indicates, that the system which ensures the vertical polarization of the beam works on a constant level.

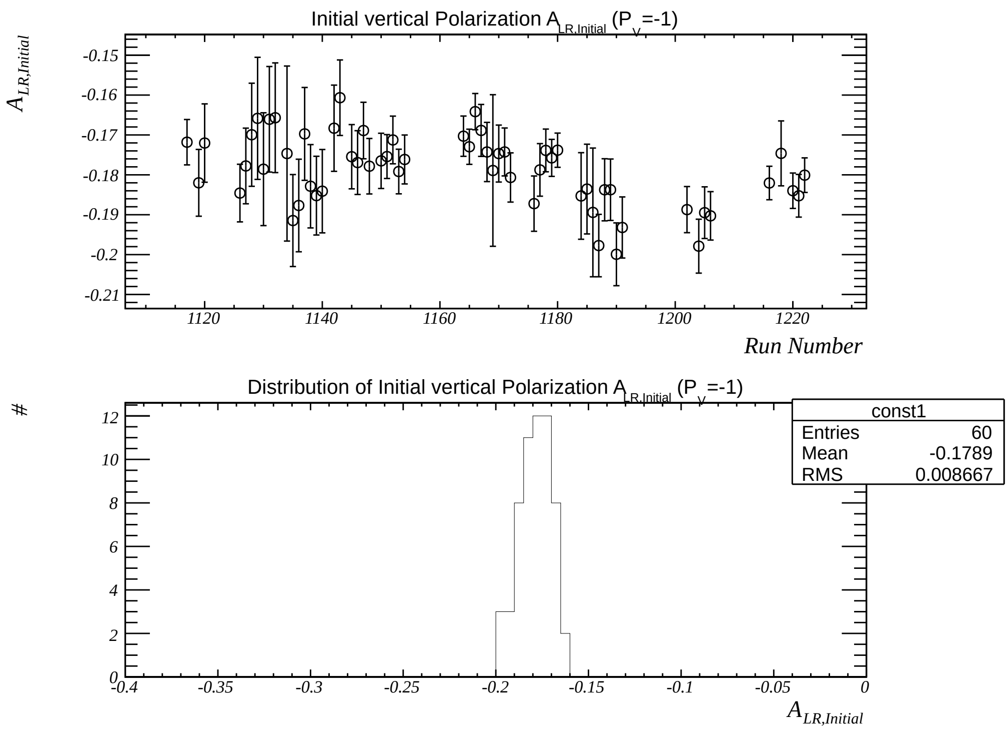

Figure 4.10: Upper panel: The initial vertical polarization of the beam is plotted against the runs. Lower panel: The distribution of the initial polarization is shown.

4.2.1 Systematics

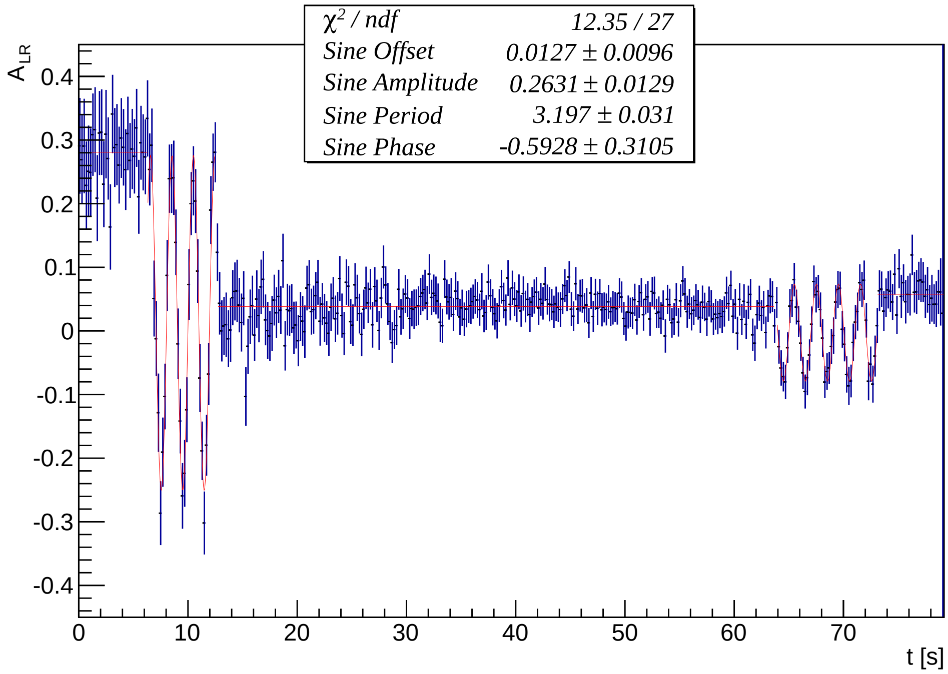

Figure 4.11: Vertical polarization fitted by sine curves for polarization state $P_V = 1$

As mentioned before, the solenoid is turned off, when the beam is completely horizontal polarized, thus the vertical polarization should vanish. However, the plot in figure 4.6 displays a small negative asymmetry after the first oscillation for polarization state $P_V = -1$. For state $P_V = 1$ this effect is inverted as shown in figure 4.11, i.e. a slightly positive asymmetry is measured after the first oscillation. Therefore the fitted sine waves are not oscillating around zero, but are shifted a little by ΔA_{LR}. The reason of a asymmetry shifted into the direction of the polarization might be a RF solenoid frequency not exactly operating on the $1 - \gamma G$ resonance. This is reasonable, because the operation point of COSY is changing and a little deviation of 0.5 Hz induces effects like this. To investigate this issue in more detail, firstly a baseline measurement for the non-polarized beam is analyzed and afterwards a cross ratio of the two polarization states is done.

Since the experiment was performed also with a non-polarized beam, the first idea is to determine an offset $\Delta A_{P_V=0}$ from this reference measurement by fitting a constant term to the asymmetry distribution (figure 4.12). Afterwards this offset is subtracted from the asymmetry measurement of the polarized beams $P_V = -1, 1$ for every run. In figure 4.12 the left-right asymmetry of a non-polarized beam is shown fitted by a constant term. Obviously the polarization is constant but shifted by an offset of

$\Delta A_{LF,P_V=0} = -0.028 \pm 0.001$. There are the following possible explanations of these shifts:

- The rate of the left detector is different from the right one, caused by uneven gains thus the thresholds are not the same.
- Geometrical reasons, i.e. the right detector is larger than the left one.
- The beam is off center to the right or traveling in a direction that is angled a bit to the right, which makes the scattering angle on the right smaller than on the left side.
- If the solenoid is not exactly operating on the spin tune frequency, the asymmetry is shifted into the direction of the polarization.

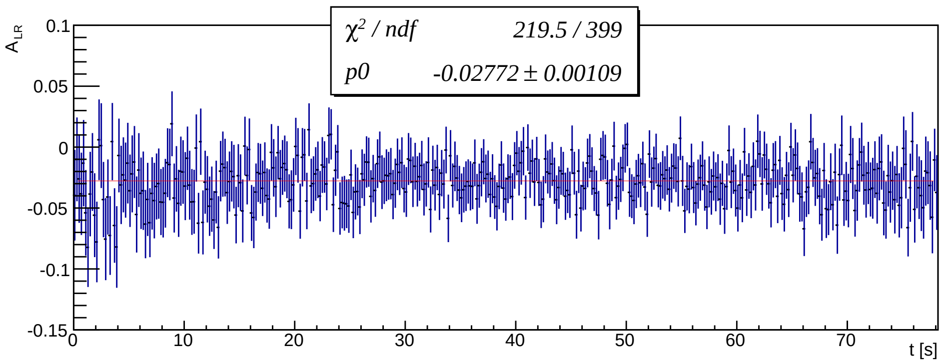

Figure 4.12: Baseline measurement of vertical polarization by fitting a asymmetry distribution of unpolarized beam $P_V = 0$.

The first issue can be reduced by calculating the asymmetry from a non-linear combination, also referred to as the cross ratio. Therefore the counting rates in the left and right detectors for beams with opposite polarization state are combined. The counting rates are given by

$$\begin{aligned} L(+) &= f^+ L_0(1 + A_L P_y^+), \\ L(-) &= f^- L_0(1 + A_L P_y^-), \\ R(+) &= f^+ R_0(1 + A_R P_y^+), \\ R(-) &= f^- R_0(1 + A_R P_y^-), \end{aligned}$$

where f^+ and f^- describe the fraction of the integrated beam luminosity for the corresponding polarization state and L_0 respectively R_0 the counts for an unpolarized beam in the left and right detector. A_R and A_L represent the analyzing power of the two detectors. From these rates, a squared ratio r^2 can be determined, where the integrated luminosity and the detector acceptance (L_0 and R_0) drops out

$$r^2 = \frac{L(-)R(+)}{L(+)R(-)} = \frac{1 + A_L P_y^- - A_R P_y^+ - A_L A_R P_y^- P_y^+}{1 + A_L P_y^+ - A_R P_y^- - A_L A_R P_y^- P_y^+}. \tag{4.11}$$

Assuming the same polarization and analyzing power of the detectors $P_y^+ = P_y^- = P_p$ and $A_L = A_R = A$, for this ratio the asymmetry can be calculated

$$\epsilon_{LR} = \frac{1-r}{1+r}, \quad \text{with} \tag{4.12}$$

$$r^2 = \left(\frac{1 + AP_y}{1 - AP_y}\right)^2 \tag{4.13}$$

$$\rightarrow \epsilon_{LR} = \frac{(1 - AP_y) - (1 + AP_y)}{(1 - AP_y) + (1 + AP_y)} = \frac{3}{2} AP_y. \tag{4.14}$$

This measure is independent of the detector acceptance and the integrated beam luminosity and will cancel out any asymmetry shifts due to different detector rates. From the asymmetries of each polarization state $P_V = 1$ and $P_V = -1$ it is possible

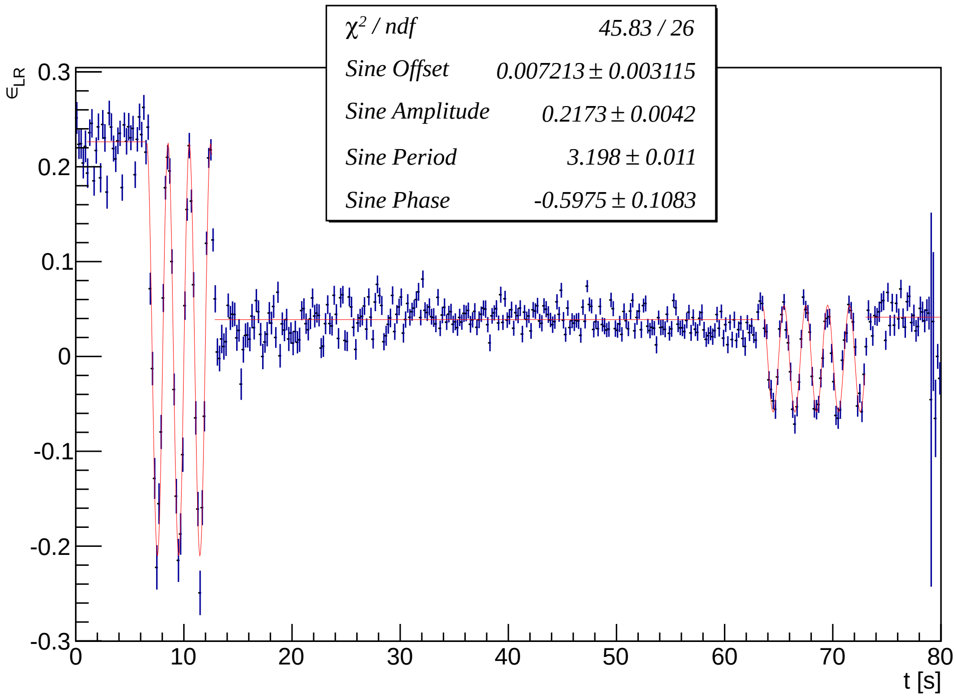

Figure 4.13: Cross ratio distribution of the vertical asymmetries $P_V = 0$ and $P_V = -1$.

to define a left-right ratio of the counting rates $\chi = \frac{L}{R}$, thus the cross ratio ϵ_{LR} is calculated by

$$r^2 = \frac{L(-)R(+)}{L(+)R(-)} = \frac{\chi_{P_V=-1}}{\chi_{P_V=1}} \tag{4.15}$$

$$\epsilon_{LR} = \frac{r-1}{r+1} \tag{4.16}$$

$$\sigma_{\epsilon_{LR}} = \frac{r}{(r+1)^2}\sqrt{\frac{\sigma^2_{\chi_{P_V=-1}}}{\chi^2_{P_V=-1}} + \frac{\sigma^2_{\chi_{P_V=1}}}{\chi^2_{P_V=1}}}, \tag{4.17}$$

whereas $\sigma_{\epsilon_{LR}}$ denotes the error of the cross ratio. In figure 4.13 the calculated cross ratio ϵ_{LR} is plotted versus the cycle time for run 1117. One sees, that the offset of the sine wave is different from zero what points to the explanation that the solenoid is off resonance. If the solenoid getting closer to the spin tune frequency, then these small offsets should all go to zero. Figure 4.14 displays for the polarization state $P_V = -1$ the offsets of the cross ratios $\Delta A_{LR,CR}$, the uncorrected asymmetry distribution $\Delta A_{LR,Unc}$ and the asymmetries corrected by the baseline measurement $\Delta A_{LR,Co}$ versus the runs. Since the expectation is a vanishing offset, values near zero represents a better resonance of the solenoid with the spin tune frequency. Therefore the corrected asymmetries (blue points) and the calculated cross ratio (black points) seems to be a good adjustment.

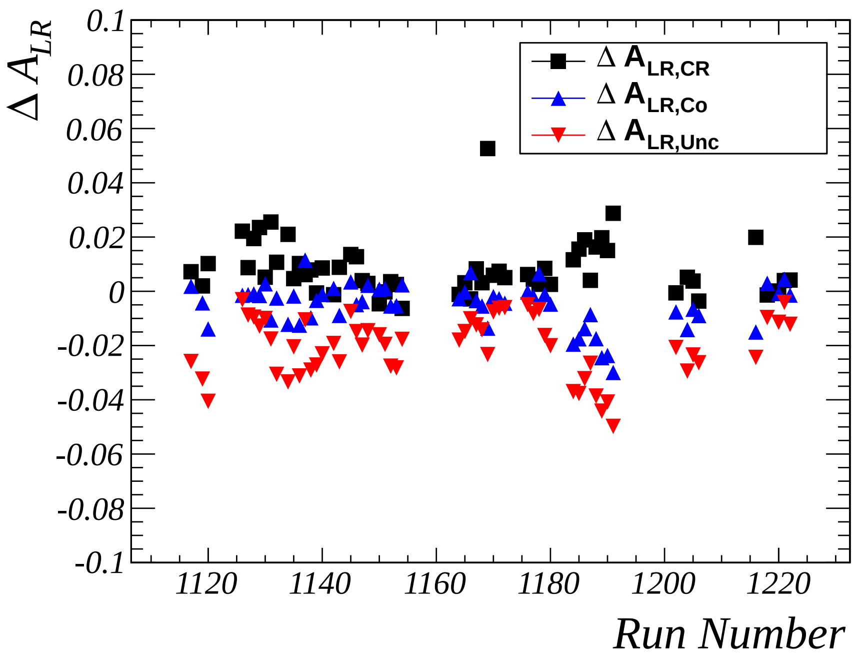

Figure 4.14: Offset of the uncorrected (red), the corrected (blue) asymmetry and the calculated cross ratio (black).

4.3 Analysis of the Horizontal Polarization

The solenoid is switched off, once the polarization is purely horizontal. Due to a high spin tune frequency of about $f_{\nu_S} = \nu_S \cdot f_{RFCosy} \approx 120\,\mathrm{kHz}$ it is not possible to measure the horizontal polarization in real time, since the event rate is too low. To solve this problem the solenoid is operating on resonance with the spin tune. The analysis method handling with this problem is presented in this section.

The spin starts to precess in the horizontal plane by an angle of $\gamma G \cdot 2\pi$ in respect to the beam momentum per turn, since the solenoid is turned off. Thus, counting the turns of the particles is equivalent of measuring the spin direction. Counting turns is started when the time stamp indicates, that the RF signal of COSY and the RF signal of the solenoid are in phase. Turn numbers N_{turns} are counted as discussed in section 4.1.1.2. The total spin precession angle is then given by

$$\Omega_{spin,total} = 2\pi\nu_S N_{turns} = 2\pi\gamma G N_{turns} \tag{4.18}$$

where $\nu_S = \gamma G = -0.160975$ is the spin tune, γ the relativistic Lorentz-factor and G the anomalous moment. The current spin phase Ω_{spin} is calculate by $\Omega_{spin,total}$ modulo 2π. For counting the events the 2π range of the spin phase is divided into nine bins $N_{bin,2\pi} = 9$ and for every signal of the four polarimeter the spin phase Ω_{Spin} is calculated, thus the content of the corresponding bin is increased by one. To find a good compromise between statistics and time resolution for the given beam conditions, this is done for a time period of $t_{bin} = 3$ seconds. At the end of the cycle for each of the 3 s time periods the up-down asymmetry is calculated according to formula 3.26 as a function of the spin phase and the result is fitted by the following function

$$f_{A_{UD},fit}(\Omega_{Spin}) = a\sin(\Omega_{Spin}) + b\cos(\Omega_{Spin}) + c, \tag{4.19}$$

where the free fit parameter are the amplitude defined as $A = \sqrt{a^2 + b^2}$, the phase $\phi_{fit} = \arctan\frac{b}{a}$ of the sine wave and c denotes a constant offset. Taking into account the signs of the phase the following arctangent definition is used

$$\arctan(a,b) = \begin{cases} \arctan(\frac{a}{b}), & b > 0 \\ \arctan(\frac{a}{b}) + \pi, & b < 0,\, a \geq 0 \\ \arctan(\frac{a}{b}) - \pi, & b < 0,\, a < 0 \end{cases} . \tag{4.20}$$

In figure 4.15 a up-down asymmetry distribution of the first time bin in a cycle is shown. Since the spin precesses during one turn in the ring by the spin tune ν_S, the up-down asymmetry A_{UD} depends on the direction of the spin vector, thus as well on the phase of this precession Ω_{Spin}, because the phase describes the angle between the spin vector and the momentum vector of the bunch. The maximal up-down asymmetry occurs, when this angle vanishes, i.e. the spin vector is parallel to the momentum vector. The relation between the up-down asymmetry and the spin phase is therefore a sine function.

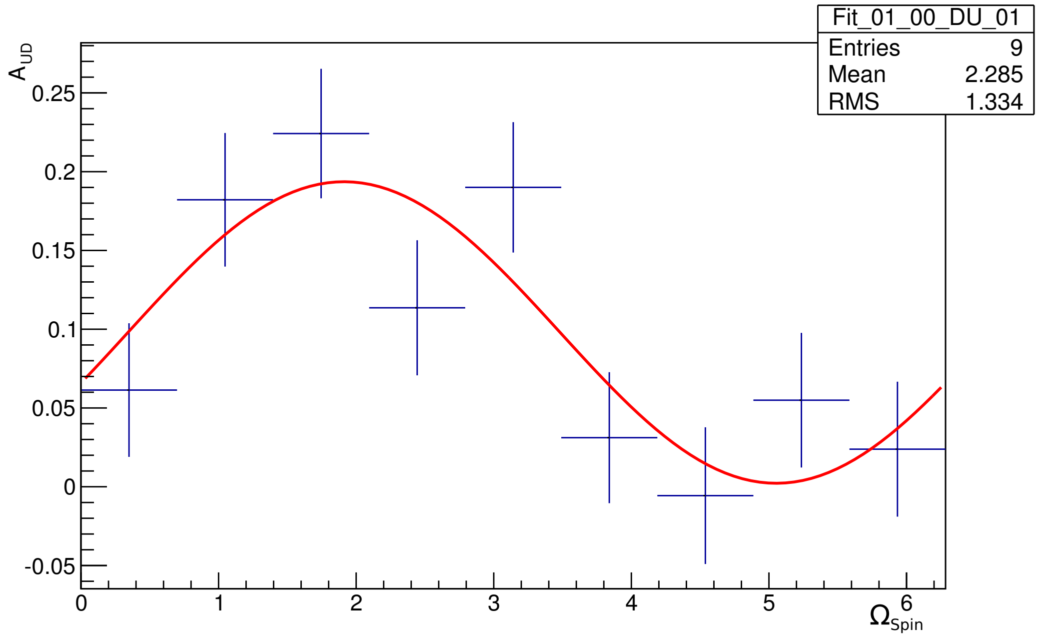

Figure 4.15: Example of an up-down asymmetry fit for one cycle. The x axis denotes the spin phase Ω_{Spin} in radiant from 0 to 2π

For each cycle the asymmetry is calculated for 17 time bins ($t_{bin} = 3\,\mathrm{s}$), thus in total for one cycle the horizontal polarization is calculated for $t_{cycle} = t_{bin} \cdot N_{timeslices} = 3\,\mathrm{s} \cdot 17 = 51$ seconds.

4.3.1 Analysis Procedure

The precision of the spin tune measurement $\nu_S = \gamma G$ needs to be at least

$$\Delta(\gamma G) = \frac{\frac{1}{N_{bin,2\pi}}}{t_{bin} \cdot f_{RFCosy} \cdot \nu_S}, \tag{4.21}$$

assuming an interval of 3 seconds measurement with a COSY RF frequency of $f_{RFCosy} \approx 750\,\mathrm{kHz}$, nine bins $N_{bin,2\pi} = 9$ within the 2π range and a spin tune of $\nu_S = -0.160975$ one gets

$$\Delta(\gamma G) = \frac{\frac{1}{9}}{3\,\mathrm{s} \cdot 750\,\mathrm{kHz} \cdot 0.160975} \approx 3 \cdot 10^{-7}. \tag{4.22}$$

The knowledge of the absolute value to the precision given above is necessary in order to make the procedure work. It is not possible to simply read the numbers from the COSY RF and the solenoid RF and extract this number with the required precision.

The most important reason is, that the two frequency generators use different clocks. Thus, in the analysis the periods for the COSY RF and the solenoid RF are measured with the same TDC. The time distributions are fitted and the results are used to calculate the spin tune by

$$\nu_{S,measured} = \gamma G = 1 - \frac{t_{RFCosy}}{t_{RFSolenoid}}. \tag{4.23}$$

As both times are measured with the same clock reference any global calibration parameters are canceling. The equation 4.23 is valid, as long as the solenoid is operating on the first negative harmonic (H=-1) of the spin tune frequency f_{ν_S}. Since the spin tune describes the angle between the beam momentum and the particle spin, the spin tune frequency is given by

$$f_{\nu_S} = \gamma G \cdot f_{RFCosy}, \tag{4.24}$$

where f_{RFCosy} denotes the orbital frequency of the beam in the storage ring. Assuming the condition of harmonic operation one gets:

$$f_{RFSolenoid} = (1 - \gamma G) \cdot f_{RFCosy} \tag{4.25}$$

$$\rightarrow \gamma G = 1 - \frac{f_{RFSolenoid}}{f_{RFCosy}} = 1 - \frac{T_{RFCosy}}{T_{RFSolenoid}}. \tag{4.26}$$

The so calculated spin tune $\nu_{S,calc}$ is taken as the central value of a range of spin tunes, which are used to calculate the asymmetry. In the analysis the range of the spin tune interval is $\pm 5 \cdot 10^{-5}$, with iteration steps of $5 \cdot 10^{-8}$. The main idea is, that hitting the correct spin tune leads to a maximization of the amplitude in the up-down asymmetry function, which corresponds to the highest polarization. In figure 4.16 a result of such a scan is shown. One sees, that the polarization passes into a clear maximum for a selected spin tune, thus for each time slice the spin tune is selected $\nu_{S,max} = \nu_{S,selected}$, which delivers the highest associated polarization. Since the phase is alternating from π to $-\pi$ the sign of the extracted amplitude parameter is scattering from plus to minus. This method provides a precision of $\sim 10^{-8}$ for the selected spin tune.

There are two practicable options of analyzing the polarization for one cycle:

- Counting the turn numbers from the phase-matching time stamp.
- Turn numbers are reseted, whenever a new time bin starts.

In the first case the start phase at the beginning of every time bin is accumulated over time, i.e. the procedure gets more and more sensitive to a variation of the spin tune. This may lead to errors at the end of the cycle, and therefore it is necessary, that the spin tune is quite stable within one cycle.
In the second case the assumption is made, that the spins are all coherent at the beginning of the time slice and previous decoherence effect only enter as common

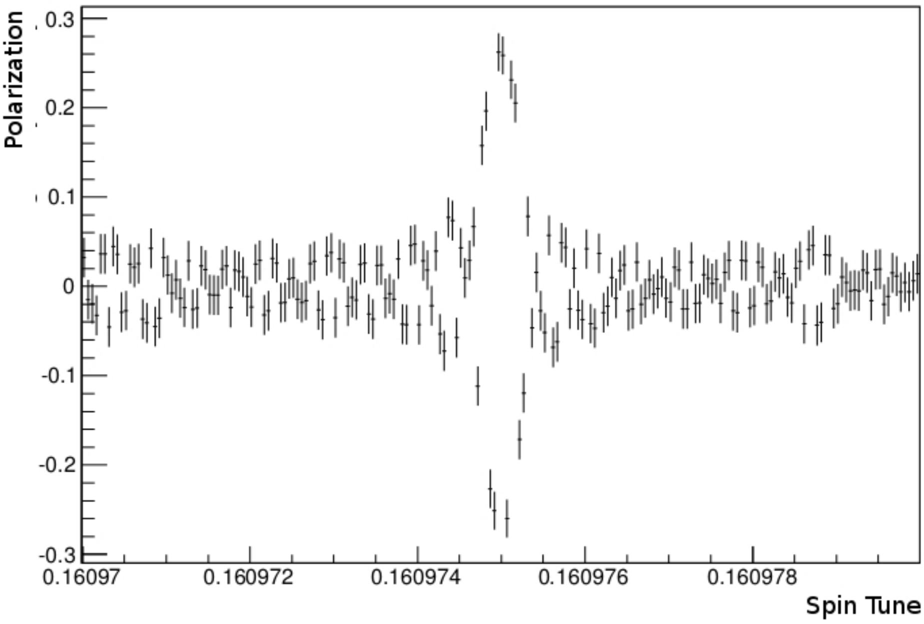

Figure 4.16: Polarization parameter a as function of the selected spin tune ν_S. It reaches the maximum close to the central value.

effect.
Although the spin tune stability was given, the second method was chosen, due to higher robustness against fluctuations of the spin tune. The consequence is, that one cannot add the statistics from different cycles directly, but that one has to analyze every cycle individually. This causes a statistical limitation in one cycle for choosing the time bins, thus the calculation of beam intensity and polarization is more crucial. The next section will describe, how this problem was handled.

4.3.2 Systematics

The method described in the section before, provides a fitted polarization value p_i for each cycle and its corresponding error σ_i. These results are added using an error weighted average:

$$p_{mean} = \frac{\sum_i \frac{p_i}{\sigma_i^2}}{\sum_i \frac{1}{\sigma_i^2}}, \tag{4.27}$$

(4.28)

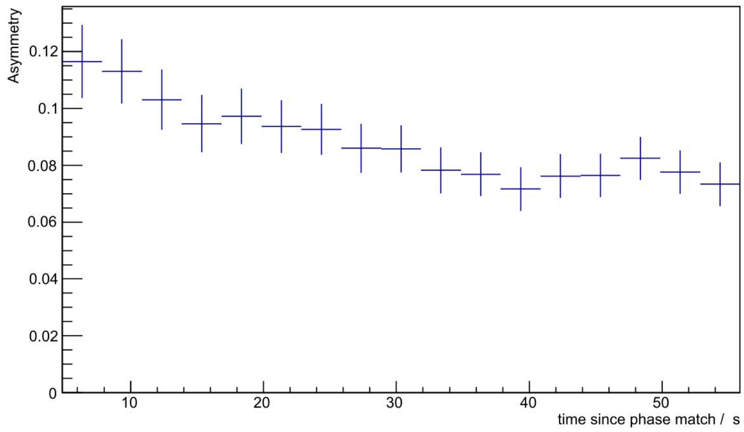

Figure 4.17: Extracted horizontal polarization for an unpolarized beam (polarization state 15)

The polarization p_i for each cycle is extracted by fitting the function 4.19 and calculating the amplitude of the this function $p_i = A = \sqrt{a^2 + b^2}$. Due to the free phase fit parameter $\phi = \arctan \frac{b}{a}$ all results are positive ($p_i = A > 0$), even in the absence of any beam polarization, thus the average polarization p_{mean} is positive, as well. This leads to a systematic offset of the polarization due to the analysis method. As a demonstration of the scope of this effect a zero measurement of the unpolarized beam (polarization state 15) is shown in figure 4.17. Due to the reduction of this effect for increasing polarizations, the correction value from the unpolarized beam cannot be used as an general offset and thus subtracted from the asymmetry measurements of the polarized beam. To handle this problem, one has to find the true polarization p_{true} by correcting the corresponding polarization given by the fit p_{fit}.

This is done by simulating a sine wave with the amplitude p_{true} smeared with a given uncertainty. For simplicity it is assumed, that the errors are Gaussian distributed and the same for all bins. Figure 4.18 shows the distribution of the fitted polarization versus the true polarization, i.e. for a given true polarization p_{true} it shows the probability distribution $w_f^{P_{true}}(p_{fit})$ for the fitted values.

Figure 4.19 shows a projection for zero true polarization $p_{true} = 0$. The fitted values are positive and within the fit errors not consistent with zero. The width of the distribution in the plot reflects the parameter error in the fit. As consequence, the fit results have to be corrected for this systematic offset caused by the experimental method. The mode (most probable value) of the distribution is at $\sigma_{bin}/\sqrt{N_{bin}}$ and

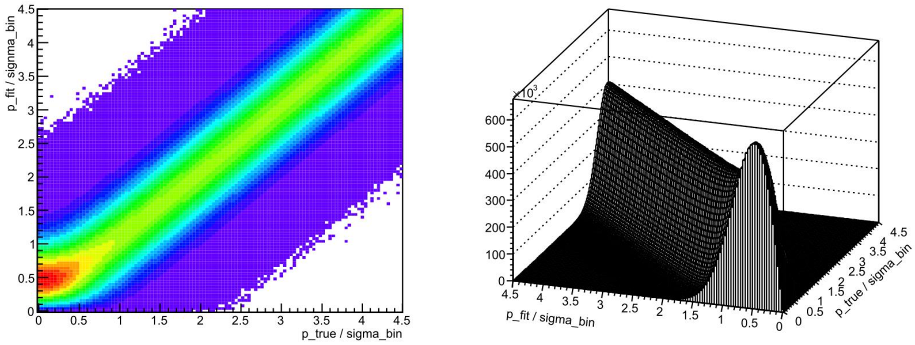

Figure 4.18: Fitted polarization p_{fit} versus true (i.e. input) polarization. The axes are normalized with respect to the error in one bin in the underlying asymmetry plot.

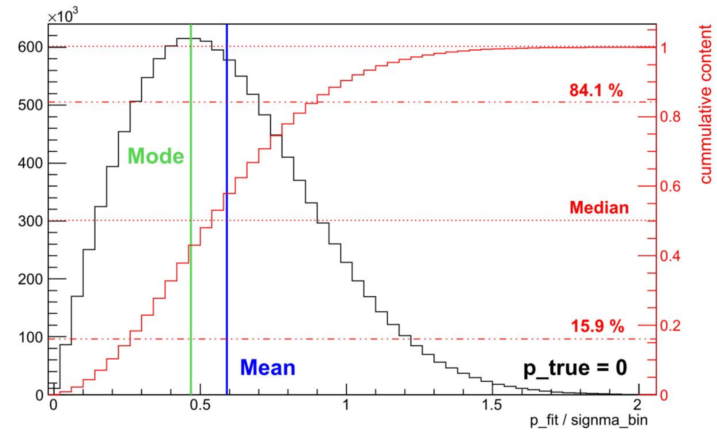

Figure 4.19: Distribution of the fitted polarization for $p_{true} = 0$, i.e. the probability distribution $w_f^{P_{true}=0}(p_{fit})$

the mean value is:

$$\langle p^0_{fit} \rangle = \frac{\sigma_{bin}}{\sqrt{N_{bin}}} \cdot \frac{\pi}{2} \tag{4.29}$$

The error for one bin can be extracted from the error for the constant value σ_c

$$\sigma_{bin} = \sigma_c \cdot \sqrt{N_{bin}}. \tag{4.30}$$

From the simulation we get the expectation mean value for the fitted polarization p_{fit} as function of the true one p_{true}. The width of these distributions should be consistent with the error of the fitted polarization $\sigma_{p_{fit}}$, which is extracted from fitting the asymmetry. As long as $p_{fit} > \langle p^0_{fit} \rangle$ is valid, there is no problem to convert the central value of the fitted polarization into an estimate for the true polarization. The challenge is the correct mapping, when the fitted value approaches the reconstruction value. This can be solved by introducing a mapping function $f(p_{true})$ which the following characteristic:

$$\overline{p_{rec}} = \overline{f^{-1}(p_{fit})} \to p_{true} \quad \text{for} \quad N \to \infty \tag{4.31}$$

Using $f(p_{true}) = \langle p_{fit} \rangle$ leads to the problem, that the function f^{-1} is only defined for $p_{fit} > \langle p^0_{fit} \rangle$. All smaller values are cut and can no longer contribute to the average:

$$\overline{p_{rec}} = \overline{f^{-1}(p_{fit} > \langle p^0_{fit} \rangle)} > p_{true} \tag{4.32}$$

Therefore, although both, the fit results as well as the original polarization, are always positive, one has to allow negative values for the reconstructed polarization p_{rec} in order to properly map the regime $p_{fit} < \langle p^0_{fit} \rangle$ and to retain a correct expectation value for p_{rec}. The analysis code provides the solution, that for all $p_{fit} < \langle p^0_{fit} \rangle$ the function f is mirrored at $(0, \langle p^0_{fit} \rangle) : f(-p) = \langle p^0_{fit} \rangle - f(p)$ in such a way, that the negative value balance the positive value to get close to the optimum: $\langle p_{rec} \rangle = p_{true}$.

4.3.3 Phase of the Asymmetry Function

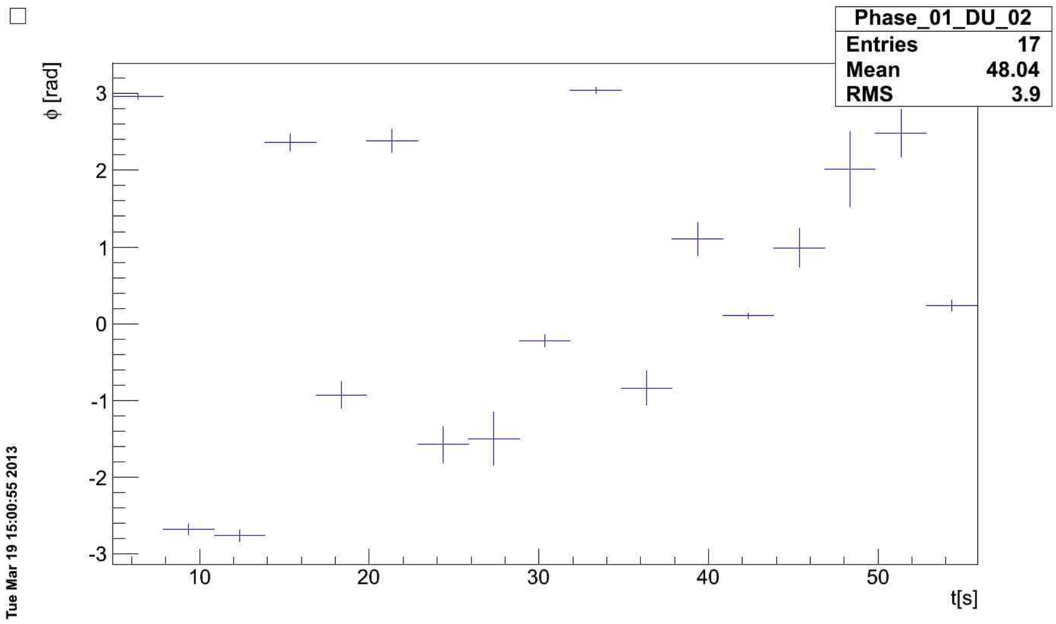

Figure 4.20: Random time distribution of the phase ϕ from the up-down asymmetry fit with selected spin tune in each time bin.

Defining the spin tune ν_S by finding the maximal up-down asymmetry in every time slice $t_{bin} = 3\,\mathrm{s}$ for each cycle provides a sensitivity of $\Delta_{\nu_s} \sim 10^{-8}$. In this case the phase $\phi = \arctan \frac{b}{a}$ of every time slice fluctuates randomly in one cycle from time bin to time bin (fig. 4.20). This indicates, that the spin tune sensitivity of this method is not high enough to match the spin tune exactly. To increase the sensitivity of the analysis, the spin tune can be fixed for the whole cycle in the ninth decimal place, which leads consequently to a sensitivity in the order of $\sigma_{\nu_s} \sim 10^{-9}$. Nevertheless, the first method is used to find an initial central value to define an interval, in which the sought-after spin tune is searched. In figure 4.21 a distribution of the phase ϕ is plotted against the cycle time t_{cycle}. One sees, that the phase alternates from around 0 to $-\pi$ and the slope is constantly decreasing from rising slightly at the beginning and decreasing faster and faster at the end of the cycle.

The error of the phase σ_ϕ is calculated from the errors of the fit by error propagation. To investigate the behavior of the phase, the distribution (figure 4.21) is fitted by a quadratic polynomial, whereas the error of the time is defined as $\sigma_{t_{cycle}} = 0$,

$$\phi_2(t) = a_2 \cdot t^2 + a_1 \cdot t + a_0, \tag{4.33}$$

where a_2 describes the quadratic coefficient of the polynomial. In figure 4.22 the time depending phase distribution fitted by the quadratic polynomial (red curve) and the fit parameters are shown. The integer value of the fixed spin tune $\nu_{S,fixed}$ (here: $= 57$)

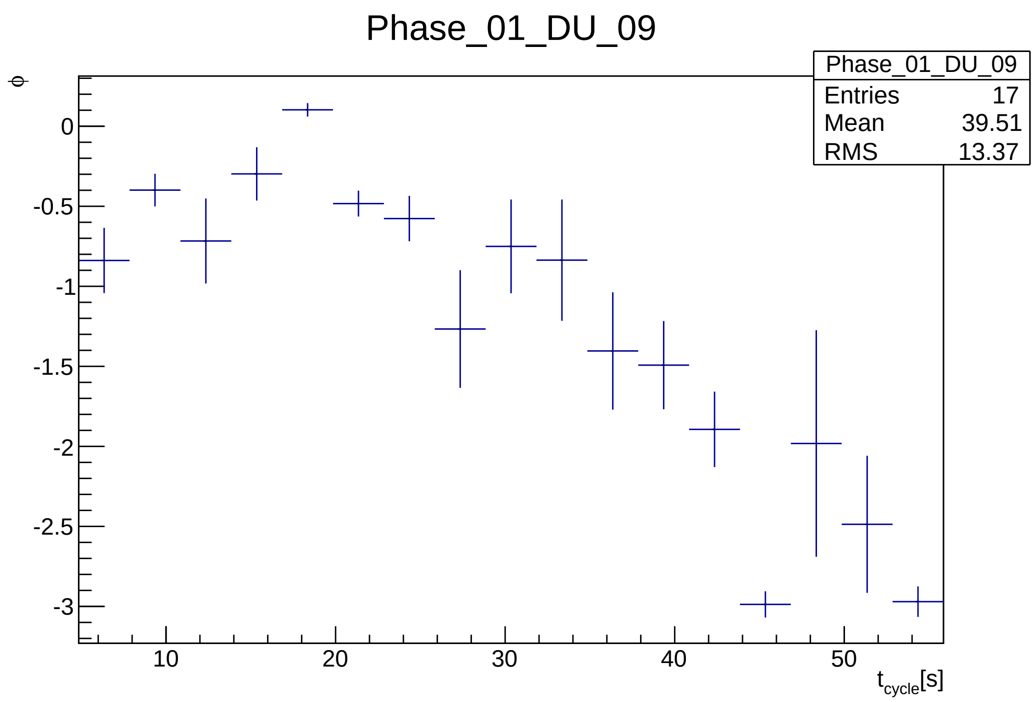

Figure 4.21: Time distribution of the phase ϕ from the up-down asymmetry fit with fixed spin tune.

run	RFSolenoid Periods [ns]	RFCosy Periods [ns]
1117-1119	1147.53973518	1332.26485549
1126-1154	1147.53955942	1332.26437085
1164-1191	1147.53718912	1332.26322190
1202-1222	1147.53637813	1332.26277431

Table 4.2: Table of the used periods of the solenoid and COSY for different runs.

has no meaning by itself, but has to be interpreted in the context of the spin tune calculated from the analysis parameter, i.e. the RFCosy and RF solenoid frequency. Since this values are changing slightly for different runs, one has to provide these frequencies to calculate the absolute spin tune ν_S. In tabular 4.2 the chosen time periods for COSY and the solenoid operating during the analysis are presented for different run intervals. Additionally one can find the calculated spin tunes used as the central value $\nu_{S,CV}$ taking into account the given frequencies. The central spin tune is calculated by

$$\nu_{S,CV} = \gamma G = 1 - \frac{T_{RFCosy}}{T_{RFSolenoid}} \tag{4.34}$$

The total spin tune is then defined as the sum of the central value and the fixed spin

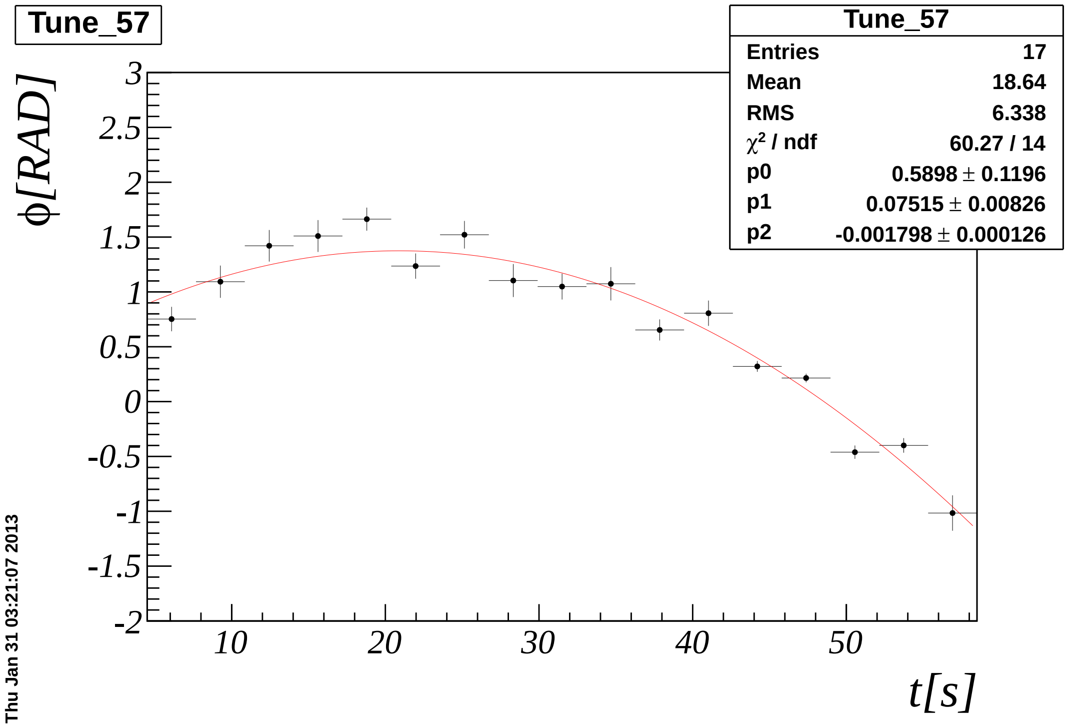

Figure 4.22: Distribution of the phase ϕ of the up-down asymmetry fit with fixed spin tune $\nu_{S,fixed} = 57$, fitted by a quadratic polynomial.

tune selected in the analysis

$$\nu_S = \nu_{S,CV} + \nu_{S,fixed} \cdot 10^{-9}. \tag{4.35}$$

As mentioned before the sensitivity of the fixed spin tune is at the order of 10^{-9}, i.e. the selected spin tune has to be multiplied by 10^{-9} to add it to the central value. Additionally, one has to consider, that the central value $\nu_{S,CV}$ represents the fixed spin tune $\nu_{S,fixed} = 50$, thus, it is necessary to subtract 50 from the selected spin tune to obtain the total spin tune ν_S .

$$\nu_S = \nu_{S,CV} + (\nu_{S,fixed} - 50) \cdot 10^{-9} \tag{4.36}$$

For different fixed spin tunes $\nu_{S,fixed}$ the time depending phase distribution is changing. The effect of changing $\nu_{S,fixed}$ is demonstrated in figure 4.23. Normally the phase is bounded in the interval $[-\pi, \pi]$, but in these plots 2π was added respectively subtracted to ϕ, whenever the phase jumps from $-\pi$ to π or vice versa. This was done to facilitate the fit procedure. The behavior of the time depending phase is discussed in the next sections, whereas firstly the linear coefficient and secondly the quadratic parameter is discussed.

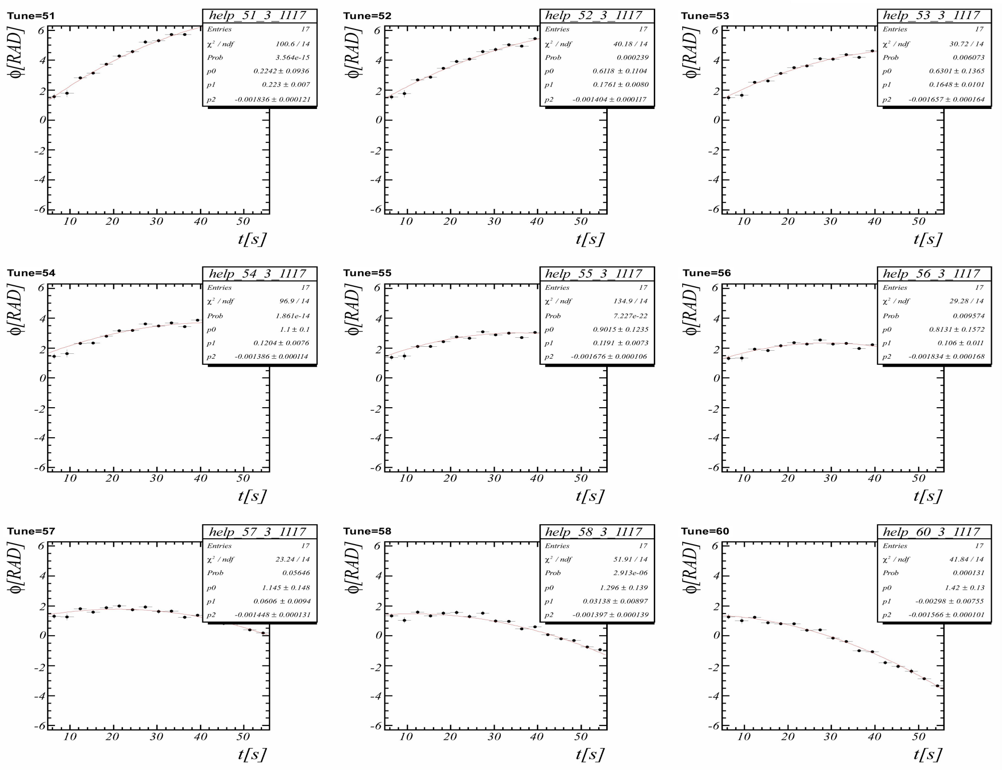

Figure 4.23: Distributions of the time depending phase ϕ for different selected fixed spin tunes $\nu_{S,fixed} = [51..60]$ (run 1117, cycle 3).

4.3.3.1 Linear Coefficient

For higher fixed spin tunes the linear slope of the quadratic polynomial fit is decreasing. This is explainable, because choosing a higher $\nu_{S,fixed}$ leads to a higher spin tune frequency used in the analysis for matching the true spin tune frequency, i.e. for positive slopes the fixed spin tune is underestimated and for higher ones $\nu_{S,fixed}$ is overestimated, respectively:

$$f_{\nu_{S,fixed}} = \nu_{S,fixed} \cdot f_{RFCosy} \tag{4.37}$$

$$\frac{\partial \phi}{\partial t} > 0 : \ \nu_{S,fixed} < \nu_{S,real} \tag{4.38}$$

$$\frac{\partial \phi}{\partial t} = 0 : \ \nu_{S,fixed} = \nu_{S,real} \tag{4.39}$$

$$\frac{\partial \phi}{\partial t} < 0 : \ \nu_{S,fixed} > \nu_{S,real}. \tag{4.40}$$

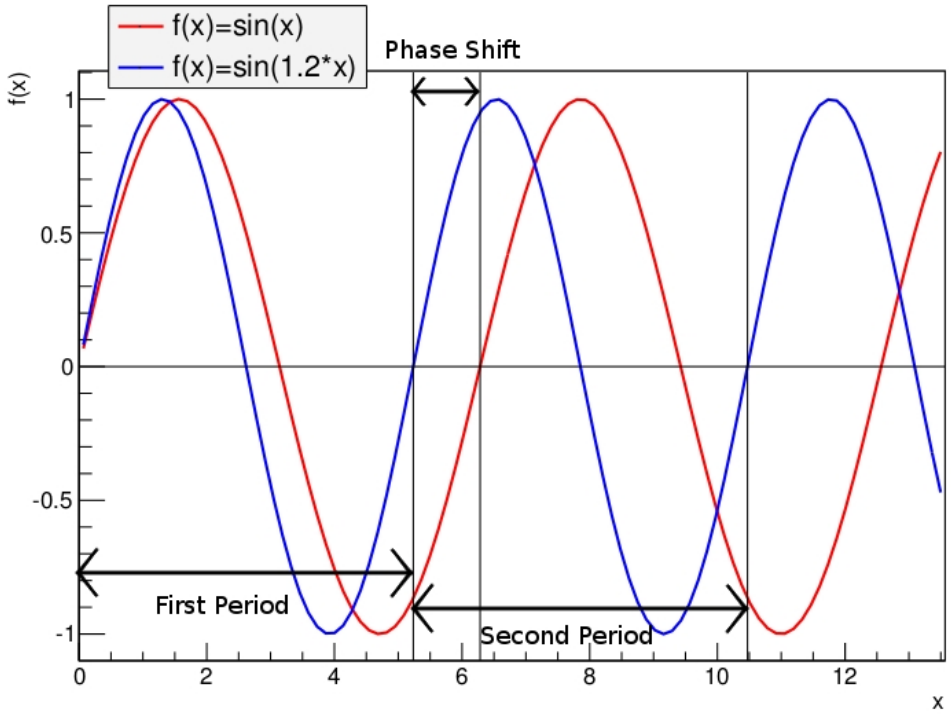

Figure 4.24: Schematic illustration of the phase shift for a higher fixed spin tune frequency (blue curve) than the true one (red curve).

If $f_{S,fixed}$ is getting higher with respect to the true frequency $f_{\nu_{true}}$, the sine waves of these frequencies would shift away from each other in this way, that the phase of the up-down asymmetry plots is reduced. That simply means, that a full period of the fixed spin tune is minor than the true spin tune period.

In figure 4.24 the phase shift is demonstrated by two sine waves. The red stands for the true spin tune frequency $f_{\nu_{true}}$, while the blue curve denotes the selected fixed spin tune frequency $f_{\nu_{S,fixed}}$. In the plot it is $f_{\nu_{S,fixed}} > f_{\nu_{true}}$, which induces a negative phase shift in the second period of the spin tune. This relation is represented by the decreasing linear slope in figure 4.23 for increasing fixed spin tunes. To find the best fixed spin tune, defined as the closest value to the true spin tune, one has to find the phase distribution, where the slope of the phase distribution fit vanishes. Therefore the linear coefficient a_1 of the quadratic polynomial fit is extracted for different selected $\nu_{S,fixed}$. Afterwards the fixed spin tune is chosen, where the linear coefficient is closest to zero.

In figure 4.25 the linear coefficient of the quadratic polynomial fit is plotted versus the selected spin tune from $\nu_{S,fixed} = 25$ to 75 for run 1117 and cycle 3. Taking into account that one run contains of about 57 cycles, i.e. for every of the three (up,down,unpolarized) polarization states $\frac{57}{3} = 19$ cycles are implemented, in every

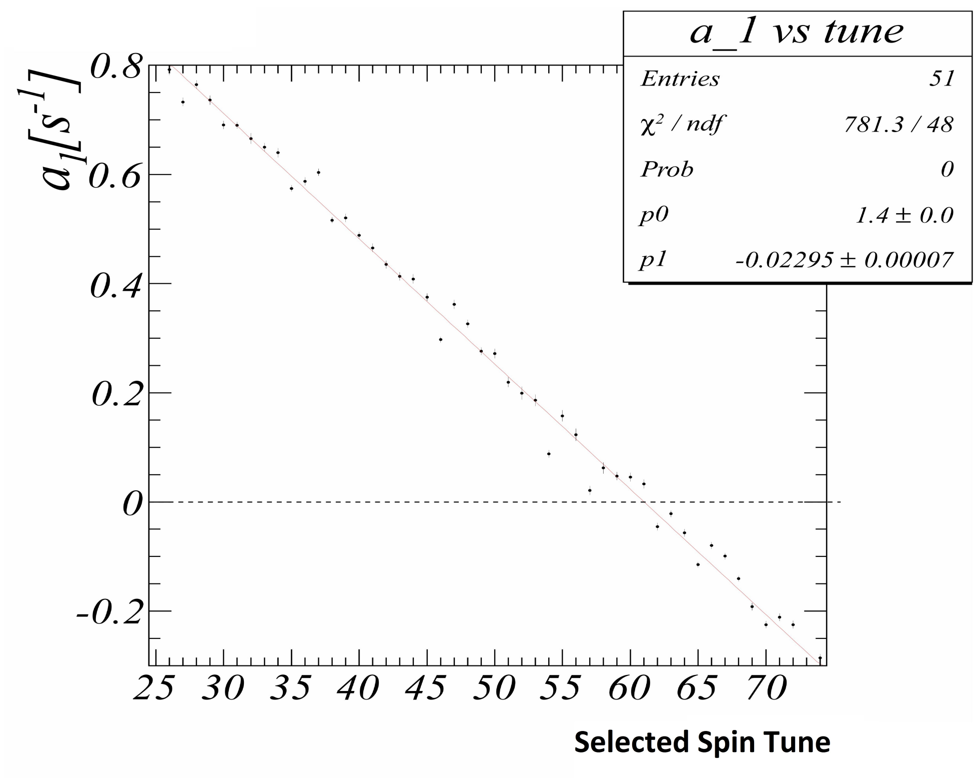

Figure 4.25: Linear coefficient of the quadratic polynomial fit versus the selected spin tune $\nu_{S,fixed} \in [25, 75]$ for run 1117 and cycle 3

run 19 quadratic polynomial fits are realized for each selected spin tune. By calculating the mean of these 19 linear fit parameters $a_{1,i}, i \in [1..19]$ it is possible to define a standard deviation, which represents the error σ_{a_1} of the distribution in figure 4.25. Due to the small error bars it is reasonable to define one linear coefficient for all cycles in one run. Additionally one sees, that the linear coefficient a_1 decreases linearly for increasing fixed spin tunes and for the fixed spin tune $\nu_{S,fixed} \approx 61$ the linear fit intercepts the x-axis, thus this value is selected for the subsequent analysis.

The outcome of this section is, that a linear slope in the phase-time diagram can be corrected in the analysis by finding the fixed spin tune for which the linear slope is closest to zero, thus the occurrence of the linear term originates from overestimating or underestimating the real spin tune.

4.3.3.2 Quadratic Coefficient

Since the phase of the up-down asymmetry fit $\phi_{A_{UD},fit}$ is not only depending on time linearly but also quadratically, in this section the quadratic coefficient a_2 is investigated. A non-linear time depending phase indicates, that the spin tune $\nu_{S,real} = \gamma G$ of the particles in the beam is changing in time. To determine the order of this phenomena, respectively on which parameter the quadratic coefficient a_2 depends, first of all, one has to extract one value per run. Afterwards these values are compared to different adjustable observables of the storage ring like the heating and the sextupole strength.

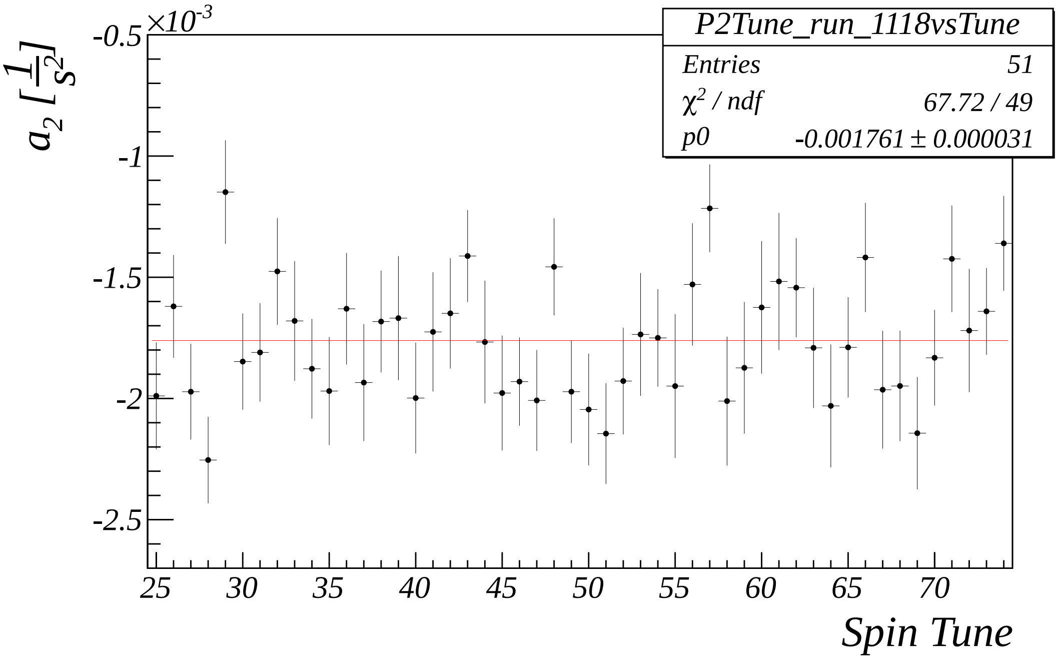

Figure 4.26: Quadratic coefficient versus fixed spin tune $\nu_{S,fixed} = [25, 75]$ for cycle 1 in run 1118 and polarization state $P_V = -1$.

Changing the selected spin tune effects only the linear term of the asymmetry fit but the quadratic coefficient stays constant for all fixed spin tunes within one cycle. This is demonstrated in figure 4.26, where the quadratic coefficients are plotted versus the selected fixed spin tune for the first cycle of run 1117 and polarization state $P_V = -1$. The error of the quadratic parameter σ_{a_2} is extracted from the fit function. One sees, that a_2 is constant for all tunes within its error and that a_2 is in the order of $-0.0015\,\frac{1}{s^2}$.

For the following investigation of a_2 the best fixed spin tune provided by the analysis in the section before is used. Since one run contains normally of about 15-19 cycles for every of the 3 polarization states, it is possible to extract several quadratic coefficients for one run. In this analysis every of the initial vertical polarization state P_V was treated independently, thus the coefficients a_2 were calculated separately for $P_V = 1$ and $P_V = -1$.

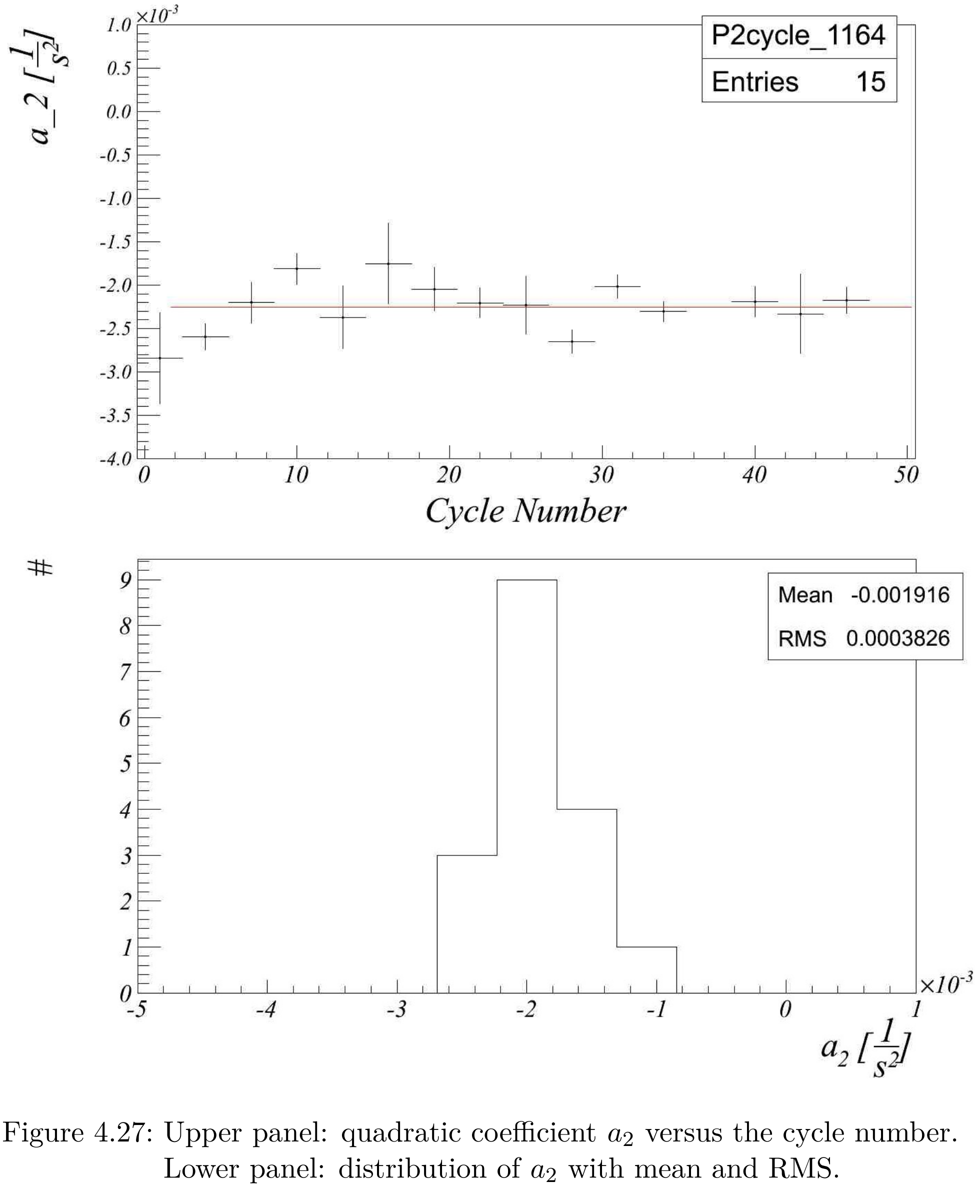

Figure 4.27: Upper panel: quadratic coefficient a_2 versus the cycle number.
Lower panel: distribution of a_2 with mean and RMS.

In figure 4.27 the upper panel illustrates, that the quadratic coefficient a_2 is constant within its error for all cycles in one run. Therefore, it is possible to define one a_2 value for each run. In the lower panel one sees the distribution of a_2 and its corresponding RMS. The mean value defines the quadratic parameter for the run and the RMS of the distribution is taken as the error. The stability of a_2 over the cycles in one run indicates, that for identical storage ring settings, namely heating and sextupole strength, the effect of the quadratically time depending phase shift is the same.

One possible explanation of the quadratic phase shift could be the method how the beam is extracted. As mentioned before, the beam was moved towards the carbon target, thus the outer particles of the beam distribution, i.e. particles with longer path length in the orbit interact firstly with the target. Since the energy of the particles depends on the path length, the spin tune varies in time. This induces a time depending phase, because a non-constant spin tune will change the phase of the asymmetry distribution of the horizontal polarization.

To estimate the effect of the quadratic phase shift one has to calculate the total phase drift $\Delta\phi_{cycle}$ during the time of one cycle $t_{cycle} = 51\,\mathrm{s}$. Assuming a quadratic coefficient of $a_2 = -2 \cdot 10^{-3}$ one gets

$$\Delta\phi_{\nu_S}(t) = a_2 \cdot t_{cycle}^2 + a_1 \cdot t + a_0 \tag{4.41}$$

$$\Delta\phi_{cycle,shift} = \Delta\phi_{\nu_S}(t = 51\,\mathrm{s}) = -0.002\,\frac{1}{\mathrm{s}^2} \cdot (51\,\mathrm{s})^2 \approx -5\,\mathrm{rad}. \tag{4.42}$$

That means, that in a time interval of 51 seconds the phase variation is minus 5 radiant. Taking into account the minimization of the linear parameter one can assume $a_1 = 0$. The time depending spin tune frequency shift is then calculated by

$$\Delta f_{\nu_S}(t) = \frac{1}{2\pi}\frac{\partial\Delta\phi_{\nu_S}}{\partial t} = \frac{1}{\pi} a_2 \cdot t \tag{4.43}$$

$$\Delta f_{\nu_S}(t = 51\mathrm{s}) = \frac{-0.002 \cdot 51\,\mathrm{s}}{\pi} \approx -0.0325\,\mathrm{Hz}, \tag{4.44}$$

which leads to a relative variation to the spin tune frequency $f_{\nu_S} = \gamma G f_{RFCosy}$ of

$$\delta_{f_{\nu_S}} = \frac{\Delta f_{\nu_S}}{f_{\nu_S}} = \frac{\Delta f_{\nu_S}}{\gamma G \cdot f_{RFCosy}} = \frac{-0.0325\,\mathrm{Hz}}{-0.1609 \cdot 750.601\,\mathrm{kHz}} \approx 2.7 \cdot 10^{-10}, \tag{4.45}$$

with a RF COSY frequency of $f_{RFCosy} = 750.106\,\mathrm{kHz}$ (run 1117-1119) and a spin tune of $\nu_S = \gamma G = -0.1609$.

Taking into account the negative sign of the phase shift, the spin tune frequency will decrease by Δf_{ν_S}. As previously explained one quadratic coefficient a_2 for every run was calculated, thus one phase shift $\Delta\phi_{shift}$ respectively one spin tune frequency shift Δf_{ν_S} for each run can be determined. In figure 4.28 Δf_{ν_S} is plotted versus the runs. One recognizes, that the values are scattering from nearly 0 Hz to 0.05 Hz and are obviously not constant over the runs. Since different runs were performed with different settings, in the next section two possible observables are presented on which the frequency shift may based on.

After all, it should be noted, that a phase shift $\Delta\phi_{cycle,shift}$ of -5 radiant provided by a fixed spin tune setting in the analysis, corresponds to a shift in the spin tune $\Delta\nu_S = \Delta\gamma G$ at the same order of the spin tune frequency shift $\delta\nu_S \approx 10^{-10}$ calculated in equation 4.45. That means, that the spin tune of the particles is changing slightly during the storage time. It is very impressing, that the analysis method provides a sensitivity to measure such small spin tune differences.

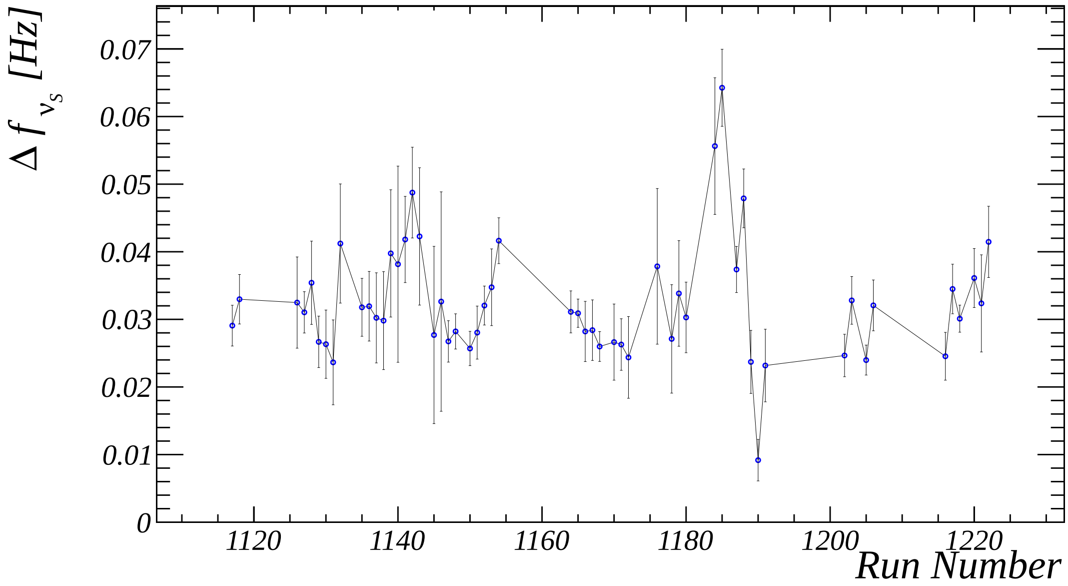

Figure 4.28: Spin tune frequency shift Δf_{ν_S} versus run number. The connection lines are plotted for a eye-friendly view.

4.3.3.3 Heating and Sextupole Strength

In the following section it is shown, how the setting of the storage ring influences the quadratic parameter a_2 respectively the phase shift. Therefore the possible dependency of two variables, namely the heating of the beam and the strength of the sextupole magnets, is discussed. As mentioned in chapter 1.2 heating the beam by a an additional dipole E-field expands the phase space of the beam by increasing the emittance, thus the lifetime of the beam reduces, due to the higher interaction rate between the beam particles and the carbon atoms of the target placed in front of the EDDA detector. Since several runs were performed with the same heating setting, one obtains multiple values for each alignment. The sorting is shown in figure 4.29, in which it is hardly visible to define any relation between heating and the spin tune frequency shift. Therefore the weighted mean of every bin and the corresponding standard deviation are calculated by

$$\Delta f^{heat}_{\nu_S,mean} = \frac{\sum_i \frac{f^{heat}_{\nu_S,i}}{\sigma^2_{f^{heat}_{\nu_S,i}}}}{\sum_i \frac{1}{\sigma^2_{f^{heat}_{\nu_S,i}}}}, \tag{4.46}$$

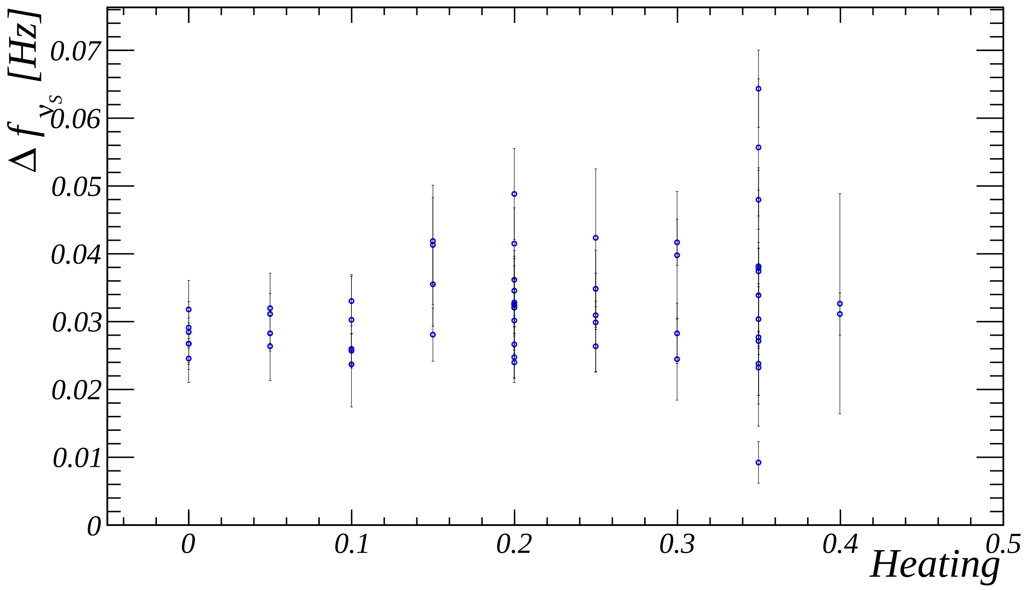

Figure 4.29: Spin tune frequency shift Δf_{ν_S} separated by the different heating values.

and

$$\sigma_{f^{heat}_{\nu_S,mean}} = \sqrt{\sum_i \frac{1}{\sigma^2_{f^{heat}_{\nu_S,i}}}}, \tag{4.47}$$

where the index heat stands for all selected heating values in the interval $[0, 0.4]$ in steps of 0.05. With this method one spin tune frequency shift $f^{heat}_{\nu_S,mean}$ is allocated to the associated heating value. The result is shown in figure 4.30, whereas the upper panel shows the weighted spin tune frequency shifts versus the heating value and the lower one displays the number of runs performed adjusting the corresponding heating, thus the error bars of the corresponding heating values in the upper plot normally decreases for a increasing number of runs with the same heating. As the upper panel shows, the spin tune frequency shift is constant within its error, that suggests a zero correlation between the heating and Δf_{ν_S} within the resolution of this analysis.

The same analysis can be done for the sextupole strength abbreviated as MXS. As mentioned in chapter 1.2, sextupole magnets are used to correct the beam chromaticity, by providing magnetic fields B_{Sext} with a quadratic field profile, thus the second derivation of B_{Sext} does not vanish.

$$B_{Sext} = \frac{1}{2}\frac{\partial^2 B_y}{\partial x^2}[(x^2 - y^2)\vec{e}_x + 2xy\vec{e}_y] \tag{4.48}$$

In this experiment four sextupoles were implemented in the storage ring where the betatron oscillation along the x-axis is separately large and the dispersion is small.

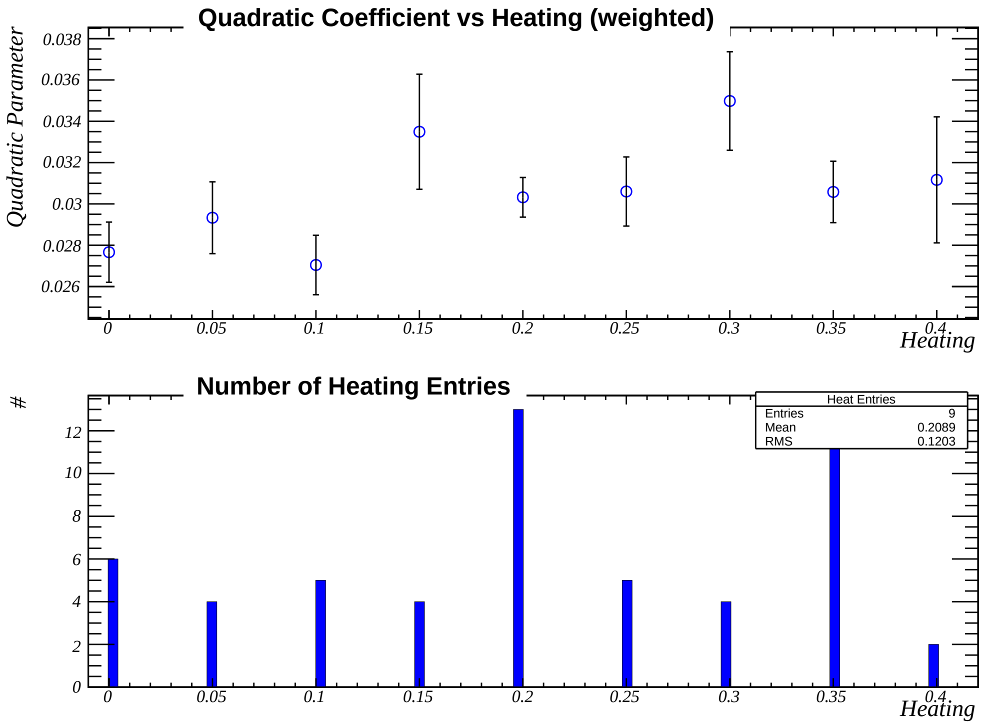

Figure 4.30: Upper panel: Weighted mean spin tune frequency shift $\Delta f_{\nu_S,mean}$ versus the heating fitted by a constant term.
Lower panel: number of runs performed with the corresponding heating.

Applying the same method as for the investigation of the heating parameter, one MXS value is given for every selected sextupole strength. The results are shown in figure 4.31, where the upper panel represents the spin tune frequency shift Δf_{ν_S} versus the MXS in percent of the maximum strength and in the lower one the number of runs performed with the respective sextupole strength are displayed. One sees, that Δf_{ν_S} is constant ($\approx 0.035\,\mathrm{Hz}$) up to the relative sextupole strength of 25% and then decreases to 0.005 Hz. Considering the low statistics for the spin tune frequency shift values at higher sextupole strength, due to the small number of runs performed with the associated setting, a potential relation between these two quantities is not secured. Additionally the investigation of two observables leads to a two dimensional problem, where a correlation between the heating and the sextupole strength will influence the results. Therefore it is reasonable to look into a series of measurement where the heating is fixed, but the sextupole strength stays variable. Accordingly the heatings with the most performed corresponding runs are chosen (heating=0.2 and =0.35) to identify the relation between Δf_{ν_S} and the applied sextupole strength (figure 4.32). For heating=0.25 it seems, that the spin tune phase shift does not change for different sextupole strengths, however for heating=0.3 a linear negative slope is observable for sextupole strength higher then 20% intercepting the x-axis near 35%.

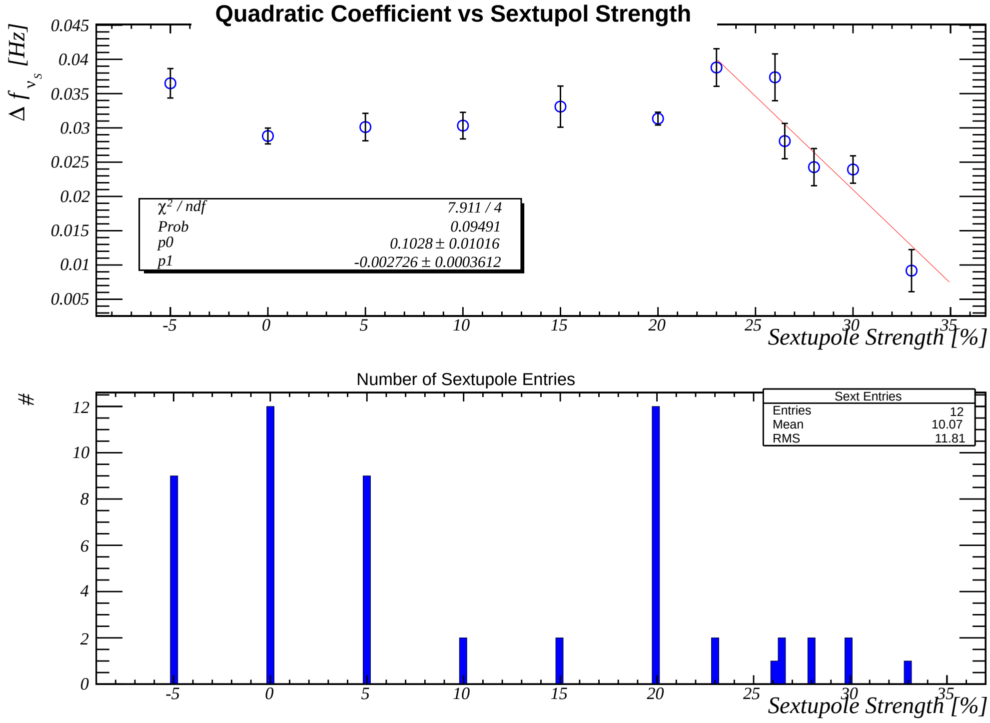

Figure 4.31: Upper panel: Weighted mean spin tune frequency shift $\Delta f_{\nu_S,mean}$ versus the sextupole strength MXS.
Lower panel: number of runs performed with the corresponding sextupole strength.

The conclusion of this section is, that the spin tune frequency shifts slightly during the storage time at the order of $0 - 0.05\,\mathrm{Hz}$, due to a phase shift of the asymmetry fits. This phase shift is depending quadratically in time, thus the frequency changes linearly:

$$\Delta f_{\nu_S}(t) = \frac{\partial \Delta\phi_{\nu_S}(t)}{\partial t} = \frac{a_2 \cdot t}{\pi} + a_1 \approx \frac{a_2 \cdot t}{\pi}, \tag{4.49}$$

where a_2 denotes the quadratic parameter of the phase distribution fit and a_1 is minimized by the method discussed in the section before. Since the spin tune is depending linearly on the Lorentz-factor $\nu_S = \gamma G$ and consequently on the particle energy $E = \gamma mc^2$, it is possible to calculate the energy distribution of the particles in the beam. Therefore it has to be clear, that the time in the cycle corresponds to a certain position in the horizontal plane of the beam. This is the case, when the beam is moving with a constant velocity into the target, which is guaranteed by the dipole magnets providing a constant B-field. For the total energy difference in a 51 second

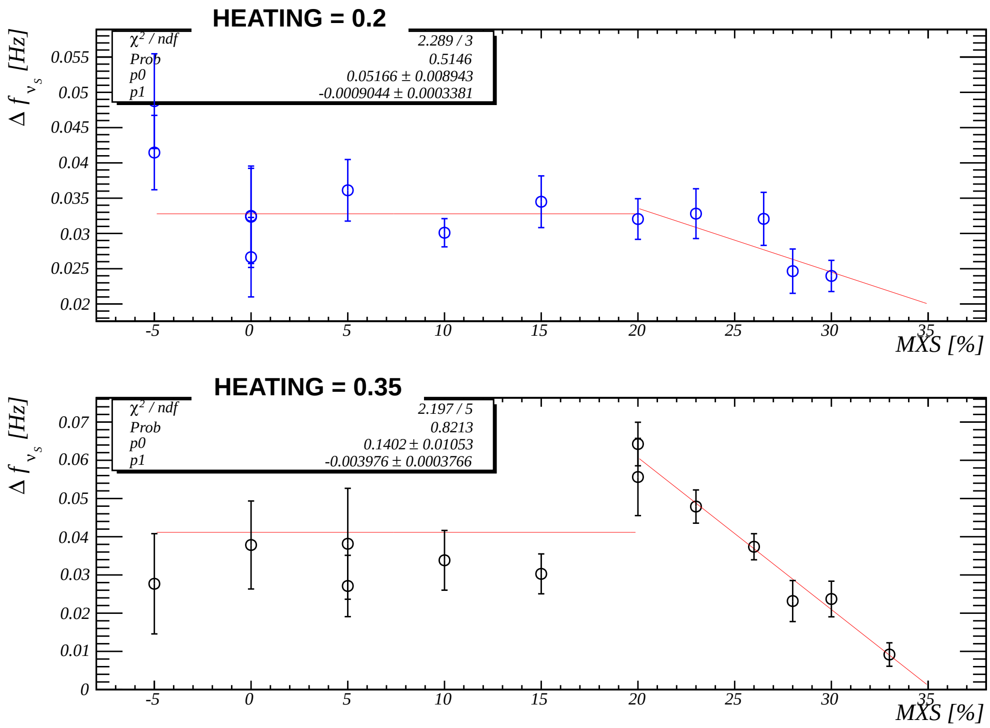

Figure 4.32: Upper panel: Δf_{ν_S} versus sextupole strength for all runs with heating=0.2. Lower panel: Δf_{ν_S} versus sextupole strength for all runs with heating=0.3.

time interval $\Delta E(\Delta t = 51\,\mathrm{s})$ one gets

$$\Delta E(t) = \Delta\gamma(t) mc^2 = \frac{\Delta \upsilon_S(t)}{G} mc^2 = \frac{\Delta f_{\nu_S}(t)}{f_{RFCosy} \cdot G} mc^2 = \frac{a_2 \cdot t \cdot mc^2}{\pi \cdot f_{RFCosy} \cdot G}, \tag{4.50}$$

$$\Delta E(t = 51\,\mathrm{s}) \approx -0.568\,\mathrm{eV}, \tag{4.51}$$

where in table 4.3 the quantities for deuterons are written down. The results represents, that particles interacting firstly with the target have higher energies than particles near the center of the beam, due to their longer path length induced by higher betatron oscillations.

Knowing the real spin tune $\nu_{S,real}(t)$ to a precision of 10^{-9} it is also possible to calculate the energy of the particles which are extracted at a certain time t to a sensitivity of 10^{-9}

$$E(t) = \frac{\upsilon_{S,real}(t)}{G} mc^2 \tag{4.52}$$

From figure 4.23 we know that a selected spin tune of 60 leads to a vanishing linear slope at the beginning of the cycle. That means, one can calculate the real spin tune

Quantity	Symbol	Value with uncertainties
Mass	m_d	1.875612793(47) GeV
Anomalous magnetic moment	$G_d = \frac{g-2}{2}$	-0.1425617692(72)
Speed of light	c	1
Cosy frequency (run 1117-1119)	f_{RFCosy}	750.6015008(1) kHz
Solenoid frequency (run 1117-1119)	$f_{RFSolenoid}$	871.4295195(1) kHz

Table 4.3: Table of quantities used to calculate the particle energy

for t=0s by

$$v_{S,real}(t = 0\,\mathrm{s}) = 1 - \frac{f_{RFSolenoid}}{f_{RFCosy}} + (60 - 50) \cdot 10^{-9} = -0.1609749328(1), \qquad (4.53)$$

which leads to a particle energy of

$$E(t = 0\,\mathrm{s}) = 2.117865435(4)\,\mathrm{GeV}, \qquad (4.54)$$

$$E_{kin}(t = 0\,\mathrm{s}) = 0.242252642(4)\,\mathrm{GeV}, \qquad (4.55)$$

$$p(t = 0\,\mathrm{s}) = 0.9835805262(5)\,\mathrm{GeV}, \qquad (4.56)$$

whereas E_{kin} denotes the kinetic energy and p the momentum of the particles extracted at t=0s. To obtain the $\frac{\Delta p}{p}$ for the time interval where the beam is in the horizontal plane one has to calculate Δp by

$$\begin{aligned}
\Delta p_{t=0,t=51} = p_{t=0} - p_{t=51} &= \sqrt{E_2^2 - m^2} - \sqrt{E_1^2 - m^2} \\
&= \sqrt{(E_1 + \Delta E)^2 - m^2} - \sqrt{E_1^2 - m^2} \\
&= \sqrt{E_1^2 + \Delta E^2 + 2E_1 \Delta E - m^2} - \sqrt{E_1^2 - m^2} \\
&= \frac{\Delta E}{\sqrt{1 - \frac{m^2}{E_1^2}}} + \sqrt{E_1^2 - m^2} - \sqrt{E_1^2 - m^2} \\
&= \frac{\Delta E}{\sqrt{1 - (\frac{m}{E})^2}} \approx 0.97\,\mathrm{eV},
\end{aligned}$$

where E_1 is the particle energy at t=0s and E_2 denotes the energy at t=51s. This result yields to a $\frac{\Delta p_{t=0,t=51}}{p}$ of approximately 10^{-9}, what represents a very low momentum spread of the particles in the beam.

4.4 Spin Coherence Time (SCT)

The main goal of the experiment in May 2012 was to investigate the spin coherence time (SCT) of a stored polarized and bunched beam in COSY. In figure 4.33 at typical plot of the horizontal polarization for a polarized beam against time is shown.

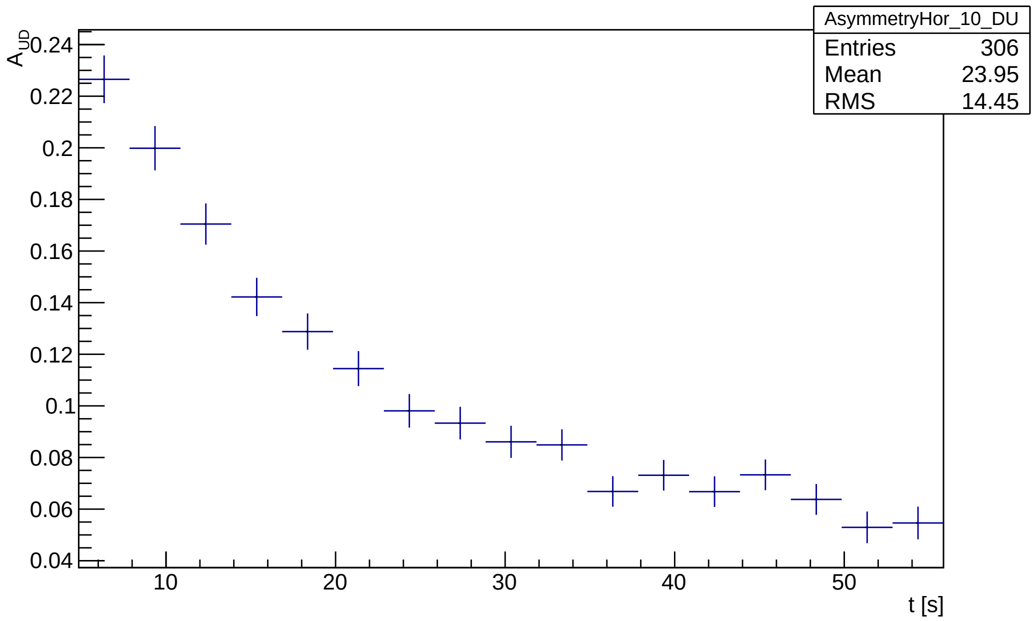

Figure 4.33: Up-down asymmetry of a polarized beam for one cycle.

The reduction of the horizontal polarization corresponds to a decoherence of the particle spins. In chapter 2.3 the SCT was introduced as the quantity describing the time where the particle spins are in phase, thus the SCT is defined as the time in which the polarization is fallen down to 60.6% of the initial polarization, a value chosen to match the Gaussian standard. To extract the SCT it is not sufficient to fit an exponential function, however one has to implement an adjustable template for the shape of the time evolution. This shape depends on the relative size of the emittance vertically and horizontally ϵ_x, ϵ_y to the beam momentum, which are two sources of changing the spin tune ν_S.

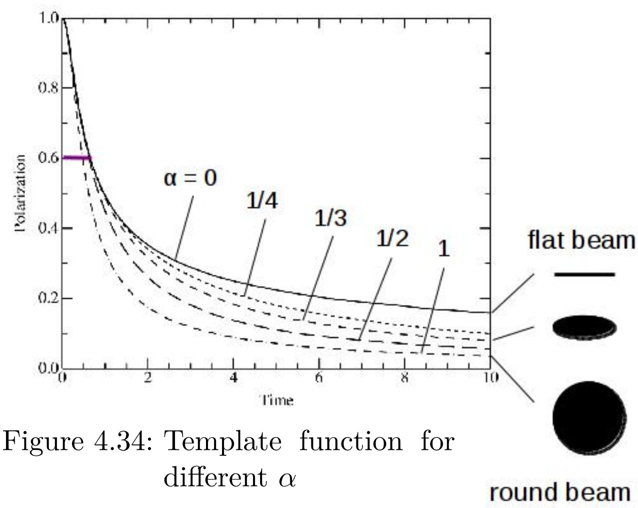

Figure 4.34: Template function for different α

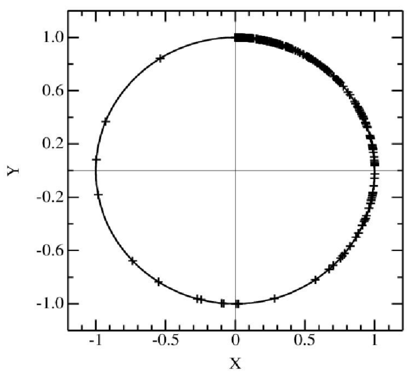

Figure 4.35: Spin distribution expanding with time

Therefore the fit function has to take into account the changing path length of the particles due to the betatron oscillations of the particles. For a bunched beam this goes with $\frac{\Delta L}{L} \propto \sqrt{\theta_x^2 + \theta_y^2}$, where $\theta_{x,y}$ denotes the angle between the particle momentum and the axis of their reference orbit. The maximum angles will follow a Gaussian distribution with the standard deviation of σ_{θ_x} and σ_{θ_y}, i.e. the beam profile depends on the ratio of the two standard deviations. For $\alpha = \frac{\sigma_{\theta_y}}{\sigma_{\theta_x}} \approx 1$ the beam has a round profile, however the beam becomes flat for $\alpha = \frac{\sigma_{\theta_y}}{\sigma_{\theta_x}} < 1$, thus the SCT will vary for different beam profiles.

A flat beam ($\alpha = 0$) provides the highest SCT, as it is shown in figure 4.34, where several simulated polarization distributions are plotted against an arbitrary time scale for different α values. The simulation was done by calculating the polarization of a spin distribution, whereas the spins are spread on a circle according to their different rotation angles in the passed turns (fig. 4.35). That is done for 2000 time points in the simulation (the reason, why the curves in figure 4.34 looks continuously) and for different α values.

The template function has to take into account the structure of the beam profile and the positivity correction discussed in chapter 4.3.2. Therefore the simulated polarization is used as a reference value for every time bin t_{TAB} in which the simulation was performed. This polarization values are stored in a table, thus the real polarization could be compared to them by finding the best fitting function, whereas an interpolation is done to obtain a continuous distribution. The fit function is defined as

$$f(t) = a_1 F_\alpha(t_{TAB}), \tag{4.57}$$

$$t_{EXP} = a_2\sqrt{1-\alpha^2}\, t_{TAB} + a_3, \tag{4.58}$$

where α describes the beam profile, a_1 represents the normalization and a_3 denotes a constant time offset defined by the experiment settings. The parameter a_2 is

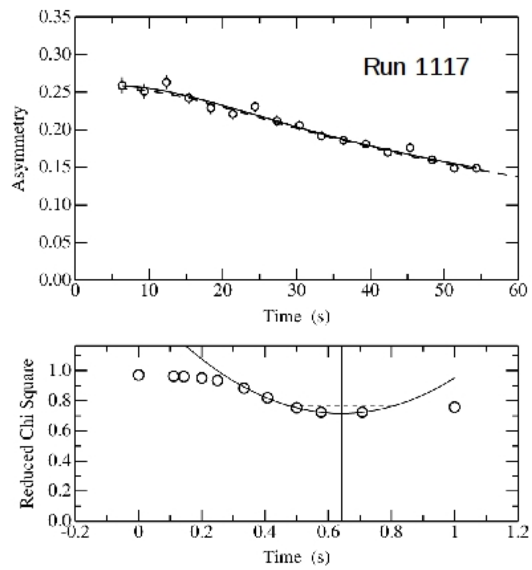

Figure 4.36: Reduced chi square for different α parameter

proportional to the spin coherence time and is obtained by adjusting the two parameters a_1 and a_2 to find the chi square minimum. In figure 4.36 the asymmetry distribution of run 1117 and its corresponding fit function is plotted. Additionally the reduced chi square for different α values is shown, whereas a quadratic curve is fitted to find the best value of α.

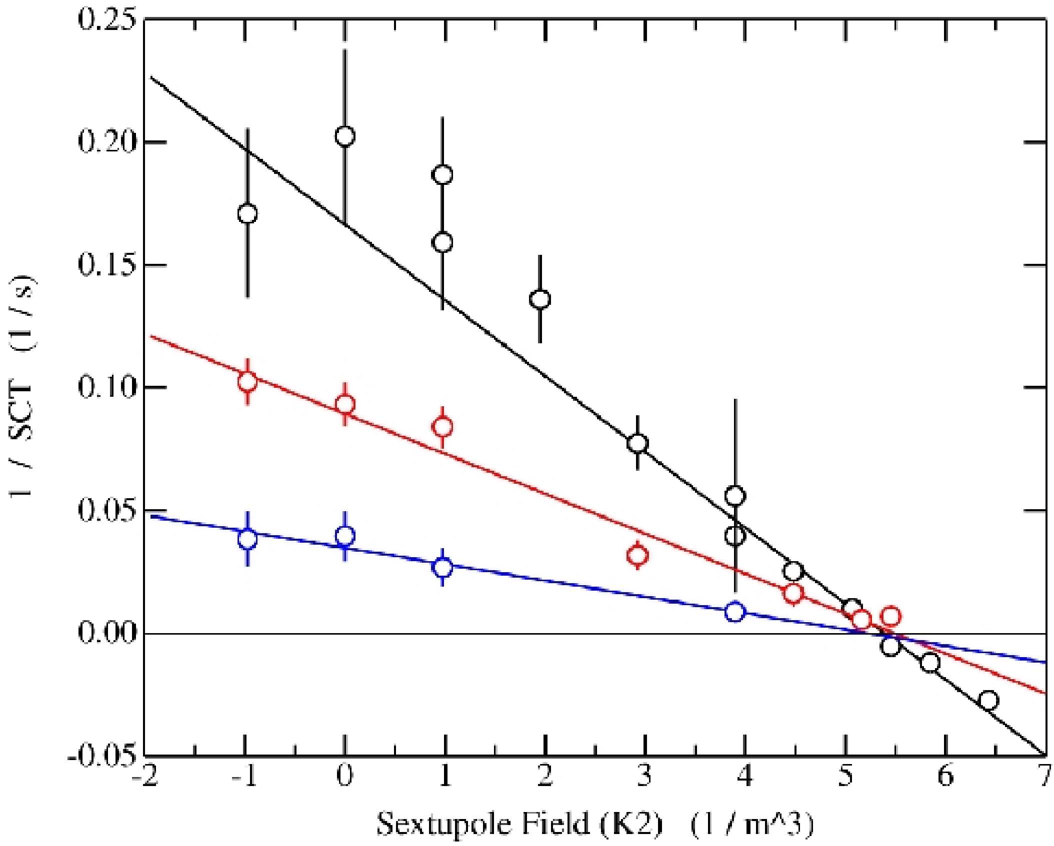

Figure 4.37: Inverse SCT against the sextupole magnetic field. The crossing point of the lines represents the best sextupole settings, thus the highest spin coherence time is reached. The different colors stands for different heating during the run

The results of the SCT measurement are shown in figure 4.37. The data were taken for three different heating settings and for several sextupole strength. One sees, that the reciprocal lifetime of the polarization decreases linearly with the inverse sextupole strength, whereas the x-axis represents the sextupole field K_2 in $\frac{1}{\mathrm{m}^3}$ with

$$K_2 = \frac{1}{B\rho} \frac{\partial^2 B}{\partial x^2} \tag{4.59}$$

whereas B is the magnetic field, ρ denotes the gyroradius of the particle. To maintain a linearity the sign of the SCT was changed for values lying behind the zero-crossing.

Since the lines are crossing the x-intercept at the same x value, one can define the a best sextupole setting, which is close to $K_2 = 5.5\,\frac{1}{\mathrm{m}^3}$. That corresponds to a sextupole strength of 28 %, which is less than the zero crossing value for the spin tune frequency shift (35%). The spin coherence time was increased to

$$\tau_{SCT,max} = 283 \pm 45\,\mathrm{s}, \tag{4.60}$$

which is a few hundred times longer than the measured SCT when the sextupoles were off or far away from the optimal sextupole settings.

Finally, it should be noted, that manipulating the beam by applying sextupole magnets can maximize the spin coherence time by a factor of several hundreds. Nevertheless, the targeted SCT is about 1000 seconds which is a factor 5 higher than the time measured during the beamtime in March 2012. Therefore several ideas were evolved, like using sextupole magnets for correcting also the chromaticity of the beam in the horizontal plane. This investigation is one part of the beamtime in February 2013 in which the JEDI collaboration will study additional systematics of a potential EDM machine.

List of Figures

List of Tables

Bibliography

[1] C.L. Bennett et al. First year Wilkinson Microwave Anisotropy Probe (WMAP) observations: Preliminary maps and basic results. *Astrophys.J.Suppl.*, 148:1, 2003.

[2] A. D. Sakharov. Violation of cp invariance, c asymmetry, and baryon asymmetry of the universe. *Journal of Experimental and Theoretical Physics*, 5:24–27, 1967.

[3] A. Czarnecki et al. Neutron electric dipole moment in the standard model: Valence quark contribution. *Phys.Rev.Lett. 78 4339-4342 hep-ph/9704355 TTP-97-10*, pages 3–4, 1997.

[4] `http://ucn.web.psi.ch/ucn_source_project.htm`.

[5] F. Rathmann A. Lehrach, J. Pretz and Y.K. Semertzidis. Storage ring electric dipole moment methods: The road to the next sensitivity level of hadronic edms. 2012.

[6] T. Ibrahim and P. Nath. Large phases and cp violation in susy. *CERN-TH Invited plenary talk at Conference: C01-06-11, p.160-167 Proceedings*, 2001-2003.

[7] V. L. Fitch R. Turlay J. H. Christenson, J. W. Cronin. Evidence for the 2π decay of the k_2^0 meson. *Physical Review Letters*, 13:138–140, 1964.

[8] H.Saoo. Measurements of cp violation in b meson decays at belle. *Belle Collaboration*, 2011.

[9] C. A. Baker, D. D. Doyle, P. Geltenbort, K. Green, M. G. D. van der Grinten, P. G. Harris, P. Iaydjiev, S. N. Ivanov, D. J. R. May, J. M. Pendlebury, J. D. Richardson, D. Shiers, and K. F. Smith. Improved experimental limit on the electric dipole moment of the neutron. *Phys. Rev. Lett.*, 97:131801, Sep 2006.

[10] M.V. Romalis, W.C. Griffith, and E.N. Fortson. A New limit on the permanent electric dipole moment of Hg-199. *Phys.Rev.Lett.*, 86:2505–2508, 2001.

[11] Y.K. Semertzidis et al. A New method for a sensitive deuteron EDM experiment. *AIP Conf.Proc.*, 698:200–204, 2004.

[12] Jorg Pretz. Measurement of Permanent Electric Dipole Moments of Charged Hadrons in Storage Rings. 2013.

[13] Andreas Lehrach, Bernd Lorentz, William Morse, Nikolai Nikolaev, and Frank

Rathmann. Precursor Experiments to Search for Permanent Electric Dipole Moments (EDMs) of Protons and Deuterons at COSY. 2012.

[14] M. E. Peskin and D. V. Schroeder. An introduction to quantum field theory. *Addison-Wesley, Reading*, page section:6.3, 1995.

[15] V. Bargmann, Louis Michel, and V. L. Telegdi. Precession of the polarization of particles moving in a homogeneous electromagnetic field. *Phys. Rev. Lett.*, 2:435–436, May 1959.

[16] Yuri F. Orlov, William M. Morse, and Yannis K. Semertzidis. Resonance method of electric-dipole-moment measurements in storage rings. *Phys.Rev.Lett.*, 96:214802, 2006.

[17] Vladimir G. Baryshevsky and Alexander J. Silenko. Potential for measurement of the tensor electric and magnetic polarizabilities of the deuteron in storage-ring experiments with polarized beams. *J.Phys.Conf.Ser.*, 295:012034, 2011.

[18] W. Pauli. Z.physik. page 601, 1927.

[19] Rijksuniversiteit Groningen Marlene da Silva e Silva. Sensitive polarimetry in a search for the deuteron electric dipole moment. 2010.

[20] Fachbereich Physik der Universität Hamburg Frank Dohrmann, Dissertation. Ergebnisse des edda-experiments zur elastischen proton-proton-streuung und studien zu deren einfluß auf streuphasenanalysen. 1997.

[21] E. Stephenson. Polarimeter and spin coherence time developments at cosy for a storage ring edm search. *PoS(STORI11)009*, 2011.